



HAL
open science

Modulation of designer biomimetic matrices for optimized differentiated intestinal epithelial cultures

Wang Xi, Jad Saleh, Ayako Yamada, Caterina Tomba, Barbara Mercier, Sébastien Janel, Tien Dang, Matis Soleilhac, Aurélie Djemat, Huiqiong Wu, et al.

► To cite this version:

Wang Xi, Jad Saleh, Ayako Yamada, Caterina Tomba, Barbara Mercier, et al.. Modulation of designer biomimetic matrices for optimized differentiated intestinal epithelial cultures. *Biomaterials*, 2022, 282, pp.121380. 10.1016/j.biomaterials.2022.121380 . hal-03598543

HAL Id: hal-03598543

<https://hal.science/hal-03598543>

Submitted on 5 Mar 2022

HAL is a multi-disciplinary open access archive for the deposit and dissemination of scientific research documents, whether they are published or not. The documents may come from teaching and research institutions in France or abroad, or from public or private research centers.

L'archive ouverte pluridisciplinaire **HAL**, est destinée au dépôt et à la diffusion de documents scientifiques de niveau recherche, publiés ou non, émanant des établissements d'enseignement et de recherche français ou étrangers, des laboratoires publics ou privés.



Modulation of designer biomimetic matrices for optimized differentiated intestinal epithelial cultures

Wang Xi^a, Jad Saleh^a, Ayako Yamada^b, Caterina Tomba^c, Barbara Mercier^a, Sébastien Janel^d, Tien Dang^a, Matis Soleilhac^a, Aurélie Djemat^e, Huiqiong Wu^a, Béatrice Romagnolo^f, Frank Lafont^d, René-Marc Mège^a, Yong Chen^b, Delphine Delacour^{a,*}

^a Cell Adhesion and Mechanics Lab, Université de Paris, CNRS, Institut Jacques Monod, F-75006, Paris, France

^b PASTEUR, Département de Chimie, École Normale Supérieure, PSL Université, Sorbonne Université, CNRS, 75005, Paris, France

^c Univ Lyon, CNRS, INSA Lyon, Ecole Centrale de Lyon, Université Claude Bernard Lyon 1, CPE Lyon, INL, UMR5270, 69622, Villeurbanne, France

^d Univ. Lille, CNRS, Inserm, CHU Lille, Institut Pasteur Lille, U1019 - UMR 9017 - CILL - Center for Infection and Immunity of Lille, F-59000, Lille, France

^e Animal Core Facility Buffon, Université de Paris, CNRS, Institut Jacques Monod, F-75006, Paris, France

^f Université de Paris, Institut Cochin, INSERM, CNRS, 75014, PARIS, France

ARTICLE INFO

Keywords:

Long-term primary cell cultures
Intestinal organoids
Substrate stiffness
3D scaffold
Tissue engineering
Epithelial differentiation

ABSTRACT

The field of intestinal biology is thirstily searching for different culture methods that complement the limitations of organoids, particularly the lack of a differentiated intestinal compartment. While being recognized as an important milestone for basic and translational biological studies, many primary cultures of intestinal epithelium (IE) rely on empirical trials using hydrogels of various stiffness, whose mechanical impact on epithelial organization remains vague until now. Here, we report the development of hydrogel scaffolds with a range of elasticities and their influence on IE expansion, organization, and differentiation. On stiff substrates (>5 kPa), mouse IE cells adopt a flat cell shape and detach in the short-term. In contrast, on soft substrates (80–500 Pa), they sustain for a long-term, pack into high density, develop columnar shape with improved apical-basal polarity and differentiation marker expression, a phenotype reminiscent of features *in vivo* mouse IE. We then developed a soft gel molding process to produce 3D Matrigel scaffolds of close-to-nature stiffness, which support and maintain a culture of mouse IE into crypt-villus architecture. Thus, the present work is up-to-date informative for the design of biomaterials for *ex vivo* intestinal models, offering self-renewal *in vitro* culture that emulates the mouse IE.

1. Introduction

The intestinal epithelium (IE), which functions as a barrier and constitutes the major site for nutrient uptake and metabolism in the small intestine, is maintained under dynamic equilibrium of cell proliferation, migration, differentiation and cell death [1]. Such a homeostatic process relies on the continuous proliferation/self-renewal of intestinal stem cells (ISCs) [2] that reside at the bottom of the tissue invaginations known as crypts. ISCs generate transit-amplifying cells that, after several rounds of division while migrating along the crypt-villus axis, differentiate mainly in absorptive enterocytes, but also

secretory cells (*i.e.*, tuft, enteroendocrine, goblet, Paneth and M cells). Altogether, these differentiated cells form a cohesive monolayer that lines the projective, finger-like villi. In contrast to the ever-youthful ISCs, the terminally differentiated cells are doomed to die as they reach the tip of the villi where they undergo cell extrusion through the so-called shedding process. Given the implication of these vital biological processes, the study of IE self-renewal and differentiation is highly informative for understanding complex biological phenomena that involve stem cell behavior, epithelial cell sorting, dynamics, organization and homeostasis, as well as pathogen defense and metabolism and thus has attracted significant research interest.

Abbreviations: AFM, atomic force microscopy; AJ, adherens junction; CL, cross-linked; DIOs, dissociated intestinal organoids; DPP-IV, dipeptidyl peptidase-IV; ECM, extracellular matrix; EDC, *N*-Ethyl-*N'*-(3-dimethylaminopropyl)carbodiimide; EM, expansion medium; FA, focal adhesion; IE, intestinal epithelium; ISC, intestinal stem cell; NHS, *N*-hydroxysuccinimide; PAA, polyacrylamide; WNR, Wnt-3A; Noggin, R-spondin.

* Corresponding author.

E-mail address: delphine.delacour@ijm.fr (D. Delacour).

<https://doi.org/10.1016/j.biomaterials.2022.121380>

Received 3 May 2021; Received in revised form 7 January 2022; Accepted 16 January 2022

Available online 18 January 2022

0142-9612/© 2022 The Authors.

Published by Elsevier Ltd.

This is an open access article under the CC BY-NC-ND license

(<http://creativecommons.org/licenses/by-nc-nd/4.0/>).

Ex vivo intestinal model systems aiming at mimicking *in vivo* tissue structure, dynamics and functions have tremendously contributed to recent advances in stem cell biology, intestinal biology and biomedical studies [3–6]. Animal models are gold standards to analyze organ structures and functions, but they are inconvenient for proper live imaging, costly and criticized for inter-individual variations, animal-human differences, and ethical problems [7]. On the other hand, intestinal cell lines, such as human Caco-2 cells, are much simpler and present numerous advantages but these cells are usually cancer-derived and lack normal physiological regulations, which concerns the maintenance of stemness, proliferation, completeness of differentiation and diversity of intestinal cell lineages [8]. The development of intestinal organoids out of ISCs has significantly advanced gastrointestinal research relevant to cell and developmental biology, physiopathology and translational biology [9]. Intestinal organoids grow either from mouse or human intestinal crypts to produce expandable and physiologically functional structures that mimic many aspects of the *in vivo* intestine organization and functions [4,10,11]. This revolutionary technology has offered an alternative to the animal models for a vast range of *in vitro* studies with accesses to close-to-physiology, live biological materials. However, intestinal organoids also present well-recognized shortcomings, including reduced and flatten “villus-like” domains as well as the closed and hard-to-reach lumen. Such small, irregular differentiated domains are mosaicked amongst the “crypt-like” protrusions and make it difficult for the study of intestinal differentiation. In addition, their culture within a tridimensional (3D) thick mass of matrix/hydrogel, usually Matrigel [4], is a limitation to applying spatially controlled gradients of biochemical and mechanical cues [12]. Hence, there is an increasing interest in culturing ISCs from organoids into epithelial monolayers on extracellular matrix (ECM) coated surfaces for intestinal biology and physiology [13–17]. Such a solution not only provides convenient access to the luminal surface by unfolding the spherical organoids into monolayers but also better controls over the mechanical and biochemical cues to the culture. It also presents the potential for further integration into a series of setups for various applications. For example, for mimicking IE morphogenesis, the substrate can be micro-engineered into a 3D architecture that guides IE into 3D crypt-villus topography [18,19]. Furthermore, when integrated into a Transwell setup, a signaling gradient can be applied to the IE monolayer to mimic the physiological distribution of secreting factors [17,18].

Nevertheless, culturing primary ISCs into renewable IE monolayers is far more difficult than culturing cell lines and requires a deep consideration of intestinal homeostatic regulatory signals. At present, cultures of primary IE on planar substrates are usually short-lived, and overcoming the limited time span is still a daunting challenge for many attempts to build an *ex vivo* intestinal model [20]. It is now known that IE homeostasis is finely regulated by the balance of many biochemical and mechanical signals [21]. For example, the morphogens Wnt, Noggin and Epidermal Growth Factor (EGF), which present decreasing gradients from the crypt towards the villus, are crucial for the maintenance of stem cell niche and promote ISC proliferation [21]. These gradients are caused by the uneven distribution of cells secreting them, such as Paneth cells located in the crypts and expressing Wnt 3 and EGF [21,22]. Besides these important biochemical cues, mechanical cues, such as ECM stiffness that rivals the potency of chemical supplements, could have a substantial influence on epithelial migration, growth, differentiation and organization [23–26]. ECM stiffness is determined by protein composition and network structure. In the gut, the spatial distribution of ECM proteins, including type IV collagen and laminins, is heterogeneous [27], thus leading to variation in ECM rigidity. For instance, the mucosa of the large intestine contains less collagen than the submucosa, indicating a stiffness gradient between these layers [28]. Similar spatio-temporal heterogeneity in ECM proteins distribution is also found in the small intestine [29,30], whereas whether there exists an ECM stiffness variation along the crypt-villus axis is yet to be determined. Changes in ECM stiffness are also associated with illness as shown for instance by

the increased macroscale stiffness associated with high ECM collagen content in the human ileum and colon of inflammatory bowel disease [25].

Recent *in vitro* investigations unraveled that substrate elasticity can dictate stem cell fate *via* regulating focal adhesions, mechano-sensing cascades as well as actomyosin-mediated contractility at cellular and tissue levels [31,32]. Conventional stiff substrates, including glass, polystyrene and polydimethylsiloxane (PDMS), do not support appropriate IE primary culture and only allow the formation of poorly organized monolayers, whereas pure Matrigel could be too soft for the formation/expansion of a spreading monolayer [33]. Alternatively, degradable polyethylene glycol (PEG) hydrogels have been proven to promote ISC proliferation at a stiffness ~ 1.3 kPa while differentiation and organoid formation were favored at a stiffness of around 190 Pa with typical cultures in Matrigel domes [34]. Together, these observations suggest a narrow mechanical window for the self-renewal, organization and differentiation of IE monolayers. Furthermore, in a theoretical framework [35], a morphogenetic alternation from columnar to squamous cell shapes in epithelial sheets could be achieved due to different force balances amongst tensions in cell-substrate adhesion, cell-cell interaction as well as apical actomyosin contractility. Even so, given the importance of substrate stiffness in regulating the cell-substrate adhesion [32], its role in determining differentiated epithelial cell shape and packing has been largely overlooked. Recent successful attempts in culturing IE monolayers include using chemically treated type I collagen substrates [18] and pure Matrigel layers laid on rigid supports [15,17]. However, these substrates are either more than one order of magnitude stiffer than the *in vivo* ECM [18,21] or employed without supportive elasticity measurement. Hence, while understanding cell-ECM interaction at different scales is a key topic in tissue morphogenesis and differentiation, how substrate mechanical properties modulate IE differentiated cell shape and organization remains unknown until now. Moreover, without such knowledge, it is difficult to design and produce designer matrices for biomimetic and tissue engineering applications.

These challenges are currently leveraged by engineering biomaterial composites of multiple pre-defined properties to recapitulate the rich yet heterogeneous biochemical and mechanical properties of the *in vivo* ECM [36]. Single component materials, such as collagens, may allow IE cell adhesion and growth [37], and rough stiffness tunability [18], but often lack other essential biochemical characteristics [20], such as laminin isoforms. Moreover, the lack of multiple niche factors in the matrices may also hinder typical IE compartmentalization, *i.e.*, the formation of large differentiated domains separated from the stem or proliferative compartments [18]. The results obtained with collagen substrates are then incomparable with many other studies using animal-extracted ECM biomaterials. Among them, the Matrigel matrix contains a wealth of diverse ECM proteins and growth factors, and in comparison with substrates of a single collagen component, it shows a higher growth efficiency for digestive tract epithelia [37,38] and allows the development of proliferative and differentiated zones [4,11,15]. Thus, Matrigel has become the gold-standard material for classical 3D intestinal organoid cultures. However, due to its low mechanical stability Matrigel may not be able to support the large expansion of IE monolayers in 2D format [15] and to our best knowledge, there was no attempt to adjust Matrigel elasticity by any means.

In this work, we aimed at creating 2D and 3D biomimetic scaffolds for IE layer growth and its proper differentiation. First, we determined the ECM elasticity of mouse small intestine along the crypt-villus axis. Based on these analyses, we then tested the influence of ECM elasticity variation on organoid monolayer expansion, organization and differentiation by developing Matrigel-based and Matrigel-coated polyacrylamide (PAA) substrates. We revealed that, according to substrate stiffness, 2D IE monolayers expanded with distinct degrees of cell shape and tissue organization, and defined an optimal range of substrate elasticity for IE differentiation. To reproduce biomimetic crypt-villus

micro-architecture of low rigidity, a simple method was further designed to mold soft gels into 3D scaffolds. We demonstrated that using this combined approach, organoid cultures could grow on soft 3D micro-fabricated substrates for several weeks and developed monolayers resembling features of the *in vivo* differentiated IE.

2. Materials and methods

2.1. Materials and chemicals

Matrigel (#734-1100), fetal bovine serum (FBS, #35-010-CV) were purchased from Corning. DMEM medium (31,966-021), Glutamax (35,050-61) are from Gibco. Advanced DMEM/F12 (#12634010), hygromycin (#10687010), penicillin and streptomycin (#15140122), geneticin (#10131027), TEMED (#17919), rabbit anti-laminin alpha-3 (#PA538937) and rabbit anti-laminin alpha-5 (#PA549930) were from ThermoFisher Scientific. The IntestiCult™ Organoid Growth Medium (#06005) was from STEMCELL Technologies, Vancouver, Canada. Solutions for making PAA gels, 40% acrylamide solution (#161-0140), 2% bis acrylamide solution (#161-0142) and ammonium persulfate (APS, #161-0700) were purchased from Bio-Rad Lab. 3-(trimethoxysilyl) propyl methacrylate (M6514), trimethylchlorosilane (TMCS, #92360), ROCK inhibitor Y-27632 (Y0503), *N*-Ethyl-*N'*-(3-dimethylaminopropyl) carbodiimide (EDC) hydrochloride (E1769), sodium deoxycholate (30,970), DNase-I (10,104,159,001), *N*-Hydroxysuccinimide (NHS) (#130672), mouse anti-collagen-IV antibody (C1926) and rabbit anti-laminin antibody (L9393) were from Sigma-Aldrich. Anti-E-cadherin mouse antibody (#610181) was from BD Biosciences (Franklin Lakes, NJ). Mouse anti-villin antibody (M3637) was from Dako. Rabbit polyclonal antibodies directed against DPP-IV (ab187048) and Na-K-ATPase (ab76020) were from Abcam (Cambridge, UK). Rabbit polyclonal antibody directed against OLFM4 (39141 S) was from Cell Signaling (Danvers, MA, USA). Rat anti-occludin was a gift from S. Robine (Institut Curie) [39]. Phalloidin-Alexa 488 (A12379), 568 (A12380) and 647 (A22287), Hoechst 33,342 for nuclear staining (H3570) were from Life Technologies. Mowiol mounting medium was homemade. Vectashield antifade mounting medium (H-1000) was from Vector Laboratories. L-WNR cells (#CRL-3276) were from ATCC.

2.2. Organoid preparation and culture

4-month old wild-type male C57/Bl6 mice were provided by the animal facility of the Institut Jacques Monod. Transgenic LifeAct-GFP mice were a gift from D. Vignjevic (Institut Curie, Paris) [40]. Mice used for intestinal crypt isolation were between 8 and 12 weeks old. After euthanasia by cervical dislocation, the small intestine was harvested, flushed with PBS to discard luminal content and cut longitudinally open. The tissue was then cut into small pieces of 3–5 mm and further washed in PBS. The pieces of intestinal tissue were then incubated on ice for 10 min in a tube containing EDTA (5 mM). The tube was then vortexed for 2 min to release the villi from the tissue. After removal of EDTA, the intestinal pieces were placed in cold PBS and vortexed vigorously for 3 min to ensure crypt release. This process is repeated 3 times, with each fraction recovered. The third and fourth fractions are usually concentrated in crypts, so these are combined and passed through a 70- μ m cell strainer to remove the remaining villi, before being centrifuged at 1000 rpm for 5 min. The pellet (crypts) were then washed in advanced DMEM/F12 and centrifuged again. These isolated crypts were used for enteroid culture as reported previously [41]. Briefly, the final pellet containing crypts is embedded in a 1:1 ratio of basal media and Matrigel, plated as 50 μ L domes in a 24-well plate and incubated at 37 °C for 20–30 min for the Matrigel to polymerize before adding the IntestiCult™ Organoid Growth Medium and the expansion medium (EM). Media was changed every 2 days and after a week the organoids were either sub-cultured or used for seeding on 2D and/or 3D scaffolds.

2.3. Preparation of expansion medium (EM)

The EM, prepared from L-WRN cells [41], was used for the expansion and growth of IE cells in the forms of organoid, 2D monolayers and 3D biomimetic cultures. Briefly, L-WRN cells were cultured with conventional DMEM medium supplemented with FBS (10% v/v), GlutaMAX (2 mM), penicillin and streptomycin (100 unit/mL). After the first day, 500 μ g/mL geneticin and 500 μ g/mL hygromycin were added into the DMEM medium to culture until confluent. The cells were then passaged and cultured with primary culture medium (PCM, advanced DMEM/F12 supplemented with penicillin (100 units/mL), streptomycin (100 μ g/mL), GlutaMAX (2 mM) and FBS (20% v/v)). The PCM supplemented with Wnt-3A, R-Spondin and Noggin produced by the L-WRN cells was collected every 24 h and mixed with fresh made PCM with a ratio of 1:1 to make EM.

2.4. Preparation of silanized glass coverslips

Silanized glass coverslips were prepared to facilitate the adhesion of polyacrylamide (PAA) hydrogel. Glass coverslips ($\varnothing = 14$ or 18 mm) were cleaned with ethanol under sonication for 5–10 min. They were then dried under airflow and activated by oxygen plasma for 5 min. During the plasma treatment, a mixture of 2% (v/v) 3-(trimethoxysilyl) propyl methacrylate and 1% (v/v) acetic acid in ethanol was prepared. The plasma-treated coverslips were then soaked in this mixture for 30 min. Then they were rinsed thoroughly with ethanol and dried under airflow. The coverslips were then baked at 120 °C for 2 h and stored at room temperature and kept dry for future use.

2.5. Production of 2D substrates

To prepare pure Matrigel 2D substrates, 50 μ L thawed Matrigel was placed on a glass coverslip ($\varnothing = 18$ mm) and spread manually to cover about 90% of the slide at 4 °C. The coverslips were then left on an event bench for 5–10 min to flatten the surface. After that, they were transferred into a 37 °C incubator and incubated for 1 h for gelation.

To produce cross-linked Matrigel (CL-Matrigel) flat substrates, a fresh-made solution of 100 mM NHS and 400 mM EDC in cold PBS (4 °C) was mixed properly with thawed pure Matrigel at a ratio of 1:10 (v/v). A drop of the mixture (50 μ L) was then spread manually on a glass coverslip ($\varnothing = 18$ mm) and flattened in a similar manner as mentioned above or by flat PAA substrates. Subsequently, the coverslips were placed in a 37 °C incubator for 2 h to form CL-Matrigel layers. The CL-Matrigel substrates were washed with PBS once and incubated in PBS at 37 °C for 24 h to remove unreacted EDC and NHS. The substrates were then stored in 1X PBS for future utilization. The recipes to produce CL-Matrigel substrates and their elasticities are presented in Table 1.

To fabricate PAA substrates with Matrigel coating, stock solutions were first prepared according to the recipe in Table 2 and stored at 4 °C. Glass coverslips ($\varnothing = 18$ mm) were properly cleaned with ethanol and treated with oxygen plasma for 5 min 60 μ L diluted Matrigel solution in Advanced DMEM/F12 (1:10, v/v) was placed on the coverslips and incubated overnight at 4 °C. The remaining solution was then discarded by pipetting to have Matrigel-coated coverslips. In the meantime, the PAA stock solutions and PBS were degassed in a vacuum chamber for 15 min. The working solution (Table 2) was quickly prepared and mixed by

Table 1
Matrigel substrates: Composition of the solutions for making Matrigel-based substrates.

	Pure Matrigel	Cross-linked Matrigel
Matrigel [μ L]	500	500
EDC [mM]	N.A.	40
NHS [mM]	N.A.	10
AFM measured elasticity [Pa]	33.3 \pm 1.6	418.8 \pm 15.2

Table 2

PAA substrates: Composition of stock and working solutions for making PAA-hydrogel substrates.

Stock solutions			
40% Acrylamide [mL]	1.25	1.25	3.75
10% Bis-acrylamide [mL]	0.3	0.5	0.75
1 × PBS [mL]	3.45	3.25	0.5
Working Solutions			
Stock solution [μL]	150	150	125
1 × PBS [μL]	347	347	372
TEMED [μL]	0.75	0.75	0.75
10% Ammonium persulfate [μL]	2.5	2.5	2.5
AFM measured elasticity	79.5 ± 3.7 [Pa]	369.2 ± 74.6 [Pa]	5.22 ± 0.64 [kPa]

vortexing for a few seconds, and a 70 μL drop was then placed on a silanized glass coverslip ($\varnothing = 14$ mm, see Section 2.4) and sandwiched by a Matrigel-coated coverslip. The set-up was left in ambient condition for 30 min to allow PAA polymerization before peeling off the Matrigel-coated coverslip from the PAA gel. As-fabricated Matrigel-coated PAA substrates were then soaked in PBS overnight to remove the unreacted chemicals before use.

2.6. Fabrication of 3D scaffolds with CL-Matrigel

2.6.1. Microfabrication of 3D negative master mold

4-inch silicon wafers and 100 μm negative photoresist dry films (Nagase ChemteX, provided by Laboratory of Analysis and Architecture of Systems (LAAS), Toulouse) were used to prepare the 3D master mold of crypt-villus architecture. Firstly, a 100 μm negative photoresist dry film was laminated on a pre-baked 4-inch silicon wafer (200 °C for 10–20 min) by a laminator at 100 °C with a speed of 0.2 m/min. This step was repeated twice more to obtain a 300 μm-thick layer of photoresist. The wafer was then exposed to UV through a chromium photo-mask with 200 μm dark dots by MJB4 mask aligner (SUSS MicroTec) for 40 s at 21.1 mW/cm². A post-exposure bake was carried out at 100 °C for 10 min on a hotplate. After, a second layer of 100 μm-thick negative photoresist dry film was laminated on the wafer as mentioned above. The wafer was exposed to UV with half of the light dose after properly aligning the second mask so that each 200 μm dot was surrounded by six 100 μm transparent circles. A similar post-exposure bake was followed and the exposed layer was developed with cyclohexanone for about 25 min on a shaker until the background surface becomes clean. After being rinsed with ethanol, the negative master mold was then dried and stored in a cool and dry place.

2.6.2. Preparation of PDMS negative mold with rounded up villi and crypts

To avoid sticking PDMS to the master mold, the mold was exposed to the vapor of TMCS for 5 min in a Petri dish before the first use. Freshly mixed PDMS polymer and linker (RTV 615, Momentive Performance Materials, 10:1 w/w) were poured on the mold. The trapped bubbles were removed by degassing in a vacuum chamber and the mixture was allowed to reticulate at 75 °C for at least 4 h. After peeling off, the first PDMS replica has villi and crypts with squared edges. The replica was then gently dipped on a coverslip ($\varnothing = 40$ mm) coated with pre-polymerized PDMS (by spin-coating at 2500 rpm for 60 s). This step transfers small drops of liquid PDMS onto the tips of villi, which formed half-spheres after hanging the structure upside down at room temperature overnight. A further incubation at 75 °C for at least 1 h was followed to fully polymerize the drops. The obtained PDMS mold was plasma treated 1 min by air plasma and exposed to the vapor of TMCS for 1 h in a sealed Petri dish, prior to being used to produce a second negative PDMS replica. After, the above steps were repeated to round up the crypts (spin-coating pre-polymerized PDMS on $\varnothing = 40$ mm coverslip at 3000 rpm for 60 s).

2.6.3. Fabrication of 3D CL-Matrigel scaffolds with villi and crypts

The negative PDMS molds from section 2.6.2 were used to prepare positive PDMS replicas with rounded villi and crypts. To produce 3D CL-Matrigel scaffolds, negative PAA molds were prepared to avoid Matrigel adhesion during molding and gelation. Briefly, after oxygen plasma treatment for 5 min, the positive PDMS mold was covered by a drop of acrylamide/bis-acrylamide working solution (for preparing PAA substrates with an elasticity of 55 kPa [42]). The trapped air bubbles were removed by vacuuming for 5 min and a silanized glass coverslip ($\varnothing = 14$ mm) was then placed on top of the working solution. The whole set-up was then transferred into a humid argon chamber to allow PAA polymerization for 1 h. The PDMS replica was then detached from the negative PAA mold that was covalently bound onto the silanized coverslip. The negative PAA mold was soaked in PBS for 48 h to reach swelling stability. A freshly made mixture of pure Matrigel and EDC/NHS (see section 2.5) was then added to the negative PAA mold and degassed under vacuum at 4 °C for 15 min before a sterile glass coverslip ($\varnothing = 14$ mm) was placed on top of the mold. Then the set-up was transferred into a humid chamber and incubated at 37 °C overnight. The formed EDC/NHS CL-Matrigel 3D scaffolds were peeled off from PAA molds and soaked into PBS for 48 h at 37 °C with multiple PBS replacements to eliminate unreacted EDC and NHS. These scaffolds were stored in PBS at 37 °C until use.

2.7. AFM measurement for the elasticity of the intestinal tissue and 2D/3D scaffolds

Mouse jejunum was dissected into 0.2–0.5 cm small pieces and cut longitudinally and transversally to get access to the luminal part of the tissue. Tissue pieces were then rinsed thoroughly with PBS for cleaning prior to atomic force microscopy (AFM) measurements.

To decellularize the intestinal tissue, the tissue pieces were carefully washed with deionized water (resistivity 18.2 MΩ/cm) on a shaker overnight at 4 °C and decellularized by incubation in 4% sodium deoxycholate while shaking for 4 h, and then with 2000 kU DNase-I in 1 M NaCl for 3 h at room temperature [43]. Although the pieces became half-transparent, crypt-villus architecture could still be distinguished under a microscope (see Fig. 1E).

For AFM measurements, the cut native intestinal tissue pieces or decellularized samples were immersed in PBS and mounted to a Petri-dish using a stainless-steel slice anchor (Warner Instruments). AFM measurements were performed by probing the surface of villi or crypts at the periphery of the tissue pieces. Similarly, the elasticity of 2D/3D CL-Matrigel/PAA scaffolds was determined by AFM under PBS.

AFM measurements were performed on a JPK NanoWizard III AFM mounted on a Zeiss Axio Observer. Z1 optical microscope, using pre-calibrated Bruker MLCT-SPH-5UM DC colloidal probes with a tip radius of 5.5 μm and calibrated according to the SNAP method. We recorded 50 μm² arrays of 8 × 8 force curves (force-mapping). Ramp size was set to 8 μm, tip velocity to 2 μm/s, and force threshold from 0.5 nN to 2 nN depending on sample elasticity to get similar indentations. Data were recorded using the JPK 6.3.43 version and analyzed using the corresponding data processing software for Hertz model fitting. Gel elasticities are shown as the mean ± S.E.M for each map (Tables 1 and 2).

2.8. Adaptation for 2D cultures and 3D scaffolds

The intestinal organoids routinely cultured in Matrigel domes were suspended in 3 mL cold Advanced DMEM/F12 and mechanically broken by repeatedly pipetting using 200 μL tips. The broken organoids were suspended in EM (section 2.3) containing 10 μM ROCK inhibitor Y-27632 and directly seeded on 2D culture scaffolds (section 2.5) or 3D scaffolds (section 2.6). These cells were allowed to attach to the scaffolds by incubating at 37 °C for 24 h and the unattached cells were washed off later. For 2D cultures, fresh EM was added to the samples. For 3D

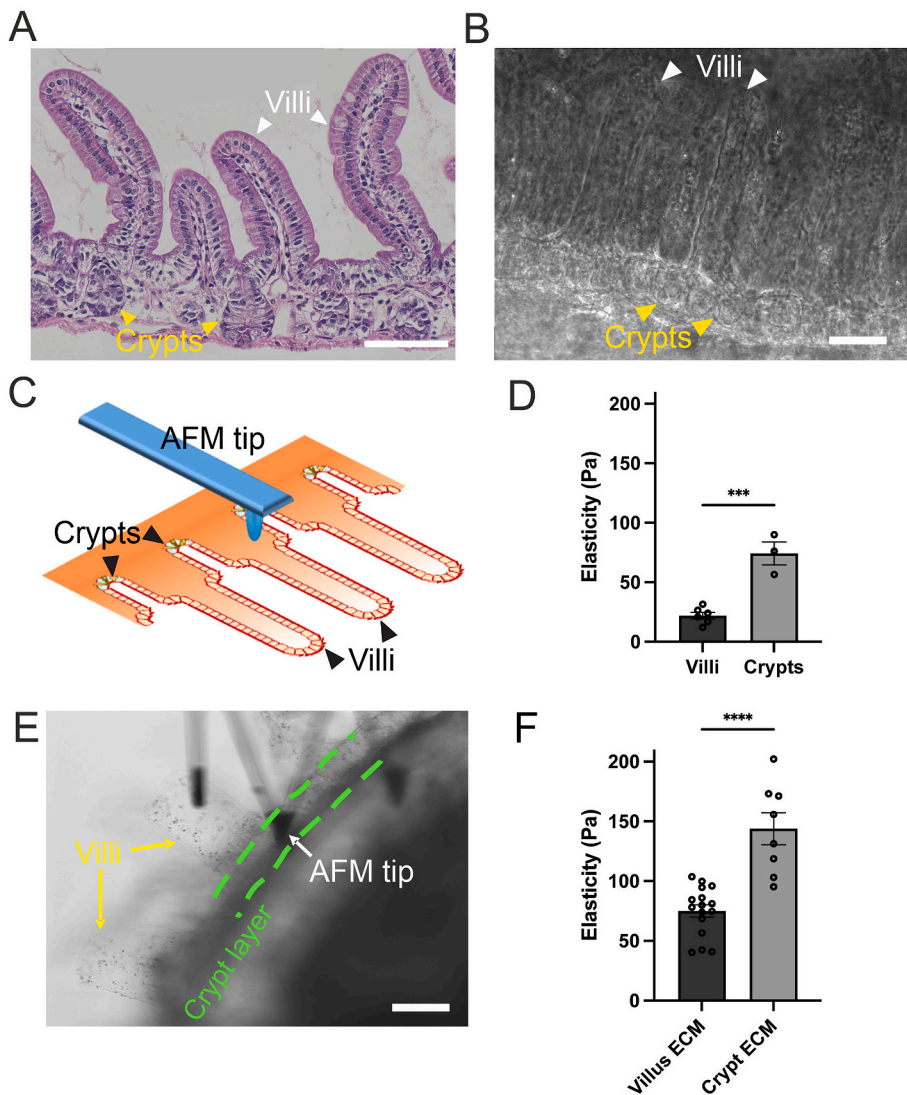


Fig. 1. Stiffness measurement along the crypt-villus axis in mouse small intestine. **A.** Histological image of hematoxylin-eosin stained paraffin section of mouse jejunum. The intestinal epithelium (IE) organizes along the crypt-villus axis. Scale bar, 100 μ m. **B.** Representative phase-contrast image of the crypt-villus axis arrangement in thin sections of fresh decellularized mouse jejunum prepared for AFM measurements. Scale bar, 100 μ m. **C.** Schematic representing the AFM approach to measuring the intestinal tissue/ECM elasticity. Scale bar, 100 μ m. **D.** Statistical analyses of the mouse jejunum IE elasticity at the villi or the crypts. Elasticity (villus) = 22.0 ± 2.8 Pa, elasticity (crypt) = 74.3 ± 9.7 Pa (mean \pm S.E. M.). $N = 2$ mouse jejunum samples, n (measured villus) = 6, n (measured crypt) = 3. Unpaired t -test: *** $p \leq 0.0002$. **E.** Representative image of live AFM measurement on a decellularized mouse jejunum sample. Crypt layer is determined by green dotted lines. Scale bar, 100 μ m. **F.** Statistical analyses of the mouse jejunum ECM elasticity at the villi and the crypts. Elasticity (ECM-villus) = 75.1 ± 5.1 Pa, elasticity (ECM-crypt) = 143.9 ± 13.3 Pa (mean \pm S.E. M.), $n = 3$ mouse jejunum samples, n (measured villus) = 16, n (measured crypt) = 8. Unpaired t -test: **** $p < 0.0001$.

cultures, cells were cultured in EM supplemented with 10 μ M Y-27632 for 12 h after seeding on scaffolds. After Y-27632 removal, cells were maintained in EM, which was renewed every two days. 3D cultures could be maintained for 3–15 weeks (the longest period tested) in these culture conditions.

2.9. Immunostainings, image acquisition and analysis

Cells were fixed using 4% paraformaldehyde for 15 min or cold methanol (-20 $^{\circ}$ C) for 5 min, permeabilized using 0.02% saponin solution in PBS for 20 min, then blocked for 30 min in 0.02% saponin/1% BSA solution in PBS before proceeding to incubation with the primary antibodies diluted in 0.02% saponin/1% BSA solution at 4 $^{\circ}$ C overnight. The secondary antibodies diluted in 0.02% saponin/1% BSA solution were then added after 3 washing steps in PBS and left to incubate for 2 h at RT. Immunostained samples were mounted in either Vectashield or Mowiol mounting media. Image acquisition was performed on a confocal LSM780 microscope (Zeiss, Zen software) or a confocal Leica SP8 microscope (STED 3D, Inerm, IPNP) with $\times 25/0.8$ NA LD LCI Plan-Apochromat, $\times 40/1.3$ NA Plan-Apochromat and $\times 63/1.2$ NA Plan-Apochromat oil/water-immersion objectives. Image analyses were performed using Imaris and Fiji.

EdU pulse was performed for proliferative cell labelling. Briefly, 10 μ M EdU in EM was incubated for 15 min. After removal of EdU

containing medium and PBS wash, cells were fixed in 4% PFA and permeabilized using 0.5% Triton X-100. Then, EdU signal was detected using the Click-iT Alexa Fluor 488 Imaging kit (Thermo Fisher Scientific).

For mouse intestinal tissue analyses, samples were prepared as previously described [44]. Briefly, 1-cm pieces of mouse small intestine were fixed for 2 h in either 4% formaldehyde or by successive 1 h incubations in cold 70%, 90%, or 100% methanol solutions and then stored at -20 $^{\circ}$ C in methanol. The samples were then paraffin-embedded and 5 μ m sections were prepared. Paraffin sections were further de-waxed in a xylene bath, rehydrated in isopropanol and in solutions with decreasing ethanol concentrations, and were processed for histological staining or immunostaining. For histology, 5 mm sections were stained with hematoxylin and eosin as previously described [45]. For immunostaining, de-waxed tissue sections were blocked in 1.5% donkey serum (Sigma-Aldrich, St Louis, Missouri, USA) for 1 h. Primary antibody incubations were performed at 4 $^{\circ}$ C overnight and secondary antibody incubations at room temperature for 2 h, both in 1.5% donkey serum solution. Hoechst 33,342 staining (Life Technologies, Paisley, UK) was used to detect nuclei. Tissue sections were mounted in home-made Mowiol 488 solution.

2.10. Statistics

All statistical analyses were performed using Prism (GraphPad Software, San Diego, CA, USA, version 7.0) and Excel (Microsoft Office). Unless otherwise stated, experiments were replicated 3 times independently.

2.11. Data availability

The data that support the findings of this study are available from the corresponding author upon request.

3. Results

3.1. Determine tissue and ECM stiffness along the small intestinal crypt-villus axis

Mechanical properties of the small intestine extracellular matrix are largely unexplored. Many measurements were obtained *via* different techniques and approaches and often reflect the rigidity of the entire intestinal mucosa [25]. For example, mechanical properties of soft tissues are measured by macro-scale testing methods, such as uniaxial tensile testing, which probes a length scale ranging from mm to cm [46]. However, key mechanical sensing events often happen within a length scale of several hundred microns. Thus, the genuine microscale stiffness of IE and its ECM remained to be determined. With an AFM probe, soft tissue can be probed down to nanometer-scale resolution, offering local tissue/ECM characteristics, to which cells respond. Along this line, to test stiffness amplitude along the crypt-villus axis in native tissue, we measured the stiffness of either villus or crypt epithelium on fresh mouse small intestine pieces using the AFM method with a micrometer-sized colloidal probe (Fig. 1A–C). We found that the average villus elasticity is 22.0 ± 2.8 Pa, and the tissue elasticity is 74.3 ± 9.7 Pa in the crypt area (Fig. 1D). Later, we decellularized intestinal tissue pieces as previously described [43] to expose the intestinal ECM. Removal of the columnar epithelial layer by chemical and enzymatic treatments preserved the underlying matrix architecture (Fig. 1B and E), enabling direct ECM elasticity measurements along the crypt-villus axis with an AFM tip (Fig. 1C and E). We found that the elasticity of the intestinal ECM is also low (75.1 ± 5.1 Pa at the villus and 143.9 ± 13.3 Pa at the crypt) (Fig. 1F). Hence, our results showed that the stiffness of mouse IE and its ECM is at least one order of magnitude lower than the values provided by previous measurements carried out on intestinal tissue as a whole [25,47]. In addition, a significant stiffness variation occurs between the crypt and villus compartments *in vivo* (Fig. 1D and F), suggesting a potential role of ECM mechanical properties in guiding ISC proliferation and differentiation. This is further in line with recent studies showing that modulation of matrix rigidity could dictate ISC fate towards stem-cell expansion or organoid formation in 3D intestinal organoid culture [34]. Based on this, we hypothesized that an ideal designer biomaterial for *ex vivo* IE culture should properly match the mechanical properties of intestinal ECM. Such soft substrates may offer a good compromise for optimal enterocytic differentiation while preserving proliferative properties of the tissue.

3.2. Cross-linked matrigel with increased elasticity supports the long-term culture of IE cells

We sought soft matrices close to the intestinal native conditions for *ex vivo* culture of IE cells. Amongst a large number of studies, researchers used Matrigel for routine intestinal organoid cultures, demonstrating the advantages of this natural hydrogel in supporting their development [4, 48]. We first determined the stiffness of Matrigel by AFM measurements and revealed a mean elasticity of 33.3 ± 1.6 Pa (Table 1), which is about 2–5 times softer than the native intestinal ECM (Fig. 1F). Second, we tested if planar, polymerized Matrigel substrates could support the

long-term culture of IE monolayers. Intestinal organoids were mechanically broken and transferred on 2D Matrigel layers on coverslips (Fig. 2A) as dissociated intestinal organoids (DIOs). While cells from organoids were initially attached to the Matrigel substrates, they could not expand to form large planar monolayers but instead grew into confined, multi-layered 3D cell domains (Fig. 2B–D). This is in line with previous reports showing that pure Matrigel could not support proper primary epithelium expansion on flat surfaces, probably in part due to the poor mechanical stability of the hydrogel [17,18,33]. Indeed, large radial Matrigel wrinkles, which might correspond to Matrigel deformation, formed around these cell domains (Fig. 2C, white arrowheads). Hence, upon cell adhesion to the substrate, traction forces generated by the cells and transduced to the adhesive sites may result in deformation on the surface of the soft gel [36], preventing further monolayer spreading. These data suggest that Matrigel does not possess appropriate mechanical stability and/or rigidity for the expansion of IE cells in 2D format. Additionally, it is known that DIOs grown on very rigid substrates such as PDMS of the same surface chemical properties quickly lose their viability and proliferative ability, resulting also in poor surface coverage [33]. Thus, these conventional materials do not allow the long-term culture of 2D IE monolayers.

We then investigated whether Matrigel could be stabilized and stiffened to match the physiological intestine ECM mechanical characteristics by increasing its cross-linking degree. We covalently crosslinked carboxylic-terminuses to amino-terminuses in a Matrigel by mixing it with a solution of EDC and NHS [18] (Fig. 2E). The course of the reactions, based on the carbodiimide crosslinking chemistry, could be slowed down at a low temperature, allowing us to flatten the pre-gelled mixture on a glass substrate before its full gelation (Fig. 2F). Newly formed amide bonds in the gel increased the cross-linking degree inside Matrigel (referred to as cross-linked Matrigel (CL-Matrigel) below) (Fig. 2E) and led to stiffened Matrigel-based hydrogel. Indeed, CL-Matrigel exhibited a 12-folds increase in the elasticity (418.8 ± 15.2 Pa) compared to the pure Matrigel (Table 1). Moreover, Matrigel surface chemistry homogeneity was maintained after the chemical cross-linking. When culturing DIOs on CL-Matrigel substrates, we found that IE domains continuously proliferated and expanded into dense monolayers which could reach a surface area of >4 mm² and nearly 100% coverage in about two weeks (Fig. 2G–I). Such IE monolayers contained large regions populated by differentiated cells such as enterocytes which developed a brush border, as demonstrated by the intense signal of apical actin and the brush border marker, villin (Fig. 2J and K, respectively). These monolayers also maintained proliferative crypt-like domains as reported previously [15] (Fig. 2K). Of note, such CL-Matrigel-based DIO cultures could be maintained as stable monolayers for a long-term (Fig. S1; the longest period tested was 70 days). Moreover, these DIO monolayers could be detached *via* conventional trypsin treatment in a typical cell passage process and re-seeded into pure Matrigel droplets or onto CL-Matrigel to form again conventional organoids or DIO monolayers, respectively, testifying to their ability of interconversion. Altogether, these data demonstrated that the combined effect of stabilization and stiffening of Matrigel allowed DIO cultures to expand into large, stable and self-renewal planar monolayers, but also promoted the emergence of enterocytic polarization and differentiation domains.

3.3. Substrate stiffness dedicates epithelial differentiated characteristics of 2D DIO monolayers

We further tested whether substrate rigidity alone was capable of influencing organization of the differentiated domains in the 2D DIO cultures. For this purpose, we produced synthetic hydrogels with tunable elasticity (Table 2) using PAA. PAA hydrogels have been used as cell culture substrates due to their univariate elasticity, with the possibility to cover a large range from 0.1 to 200 kPa [32] and to be functionalized with biomaterials by surface chemistry approaches, such as

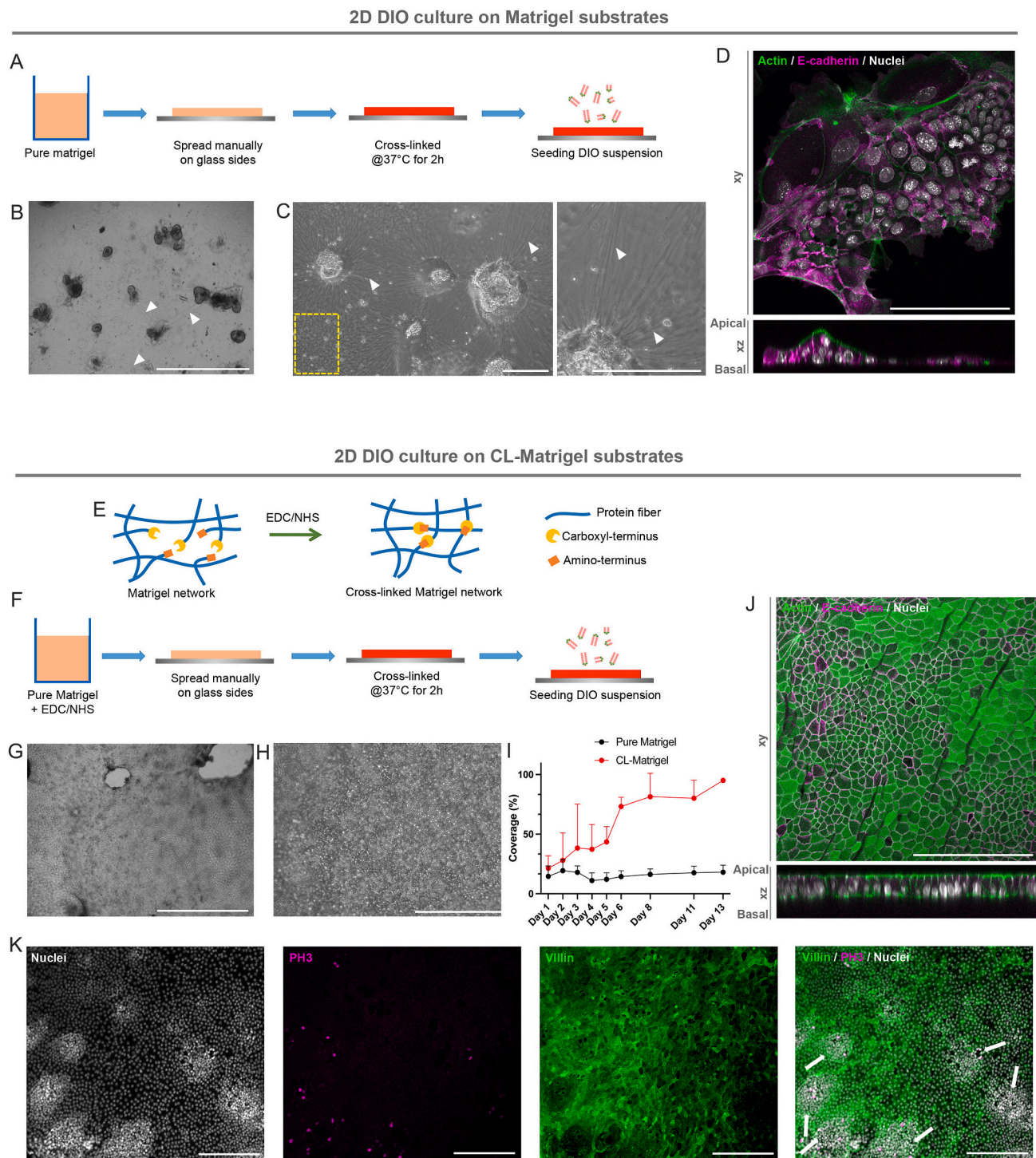


Fig. 2. Long-term culture of dissociated intestinal organoids (DIOs) on 2D Matrigel substrates. **A.** Schematic showing the preparation of Matrigel-layer coated coverslips. Thawed Matrigel was manually smeared on glass-coverslips and cross-linked at 37 °C before cell seeding. **B–C.** Bright-field images of DIOs after 9 days of culture on 2D Matrigel substrates. Yellow dashed box indicates an unmodified region of Matrigel substrate. White arrowheads indicate aligned Matrigel fibers caused by cell contractility. Scale bars, 1000 μm (**B**) and 400 μm (**C**). **D.** Confocal analysis of the distribution of E-cadherin (magenta) and actin (green) in DIOs cultured on 2D Matrigel substrates. Both *xy* (upper panels) and *xz* (lower panels) views are presented. Nuclei are stained with Hoechst 33,342 (gray). Scale bar, 100 μm. **E.** Illustration demonstrates the principle of EDC/NHS induced cross-linking in Matrigel. Cross-linking degree in Matrigel was increased by EDC/NHS treatment that covalently crosslinked carboxylic-terminuses to amino-terminuses. **F.** Schematic shows the procedure for the preparation of cross-linked (CL)-Matrigel substrates. A solution of Matrigel containing EDC and NHS was prepared and manually spread on glass coverslips. This layer was left at 37 °C for 2 h to form CL-Matrigel layer for cell seeding. **G–H.** Bright-field images of DIO culture after 35 days of culture on flat CL-Matrigel substrates. Scale bars, 1000 μm (**G**) and 200 μm (**H**). **I.** Quantitative analysis of the coverage of DIOs cultured on pure or CL-Matrigel as a function of time. Three independent experiments were carried out. Values are mean ± S.E.M. Between 2 and 9 samples were used for each condition. **J.** Confocal analysis of the distribution of E-cadherin (magenta) and actin (green) in DIOs cultured after 9 days on 2D CL-Matrigel substrates. Both *xy* (upper panels) and *xz* (lower panels) views are presented. Nuclei were stained with Hoechst 33,342 (gray). Scale bar, 100 μm. **K.** Confocal analysis of the distribution of villin (green) and phosphor-histone H3 (PH3, magenta) in 2D DIO monolayer cultured after 9 days on CL-Matrigel. White arrows point towards crypt-like areas. Nuclei were stained with Hoechst 33,342 (gray). Scale bars, 100 μm.

N-hydroxysuccinimide ester reaction [49], to promote cell adhesion. Here, based on previous reports [42], we developed solution recipes to adjust the elasticity of PAA hydrogels to overlap with the range of the *in vivo* intestinal ECM stiffness (Table 2, Fig. 1F). The PAA gels were then co-polymerized with a thin layer of Matrigel to create a Matrigel coating

on their surface (Fig. 3A, referred to as PAA-Matrigel from now on), thereby allowing stable cell-substrate adhesion.

First, we compared the early progression of tissue expansion according to various substrate rigidities, *i.e.*, 80 and 370 Pa PAA-Matrigel, CL-Matrigel (*ca.* 420 Pa) and 5.2 kPa PAA-Matrigel. We found that the

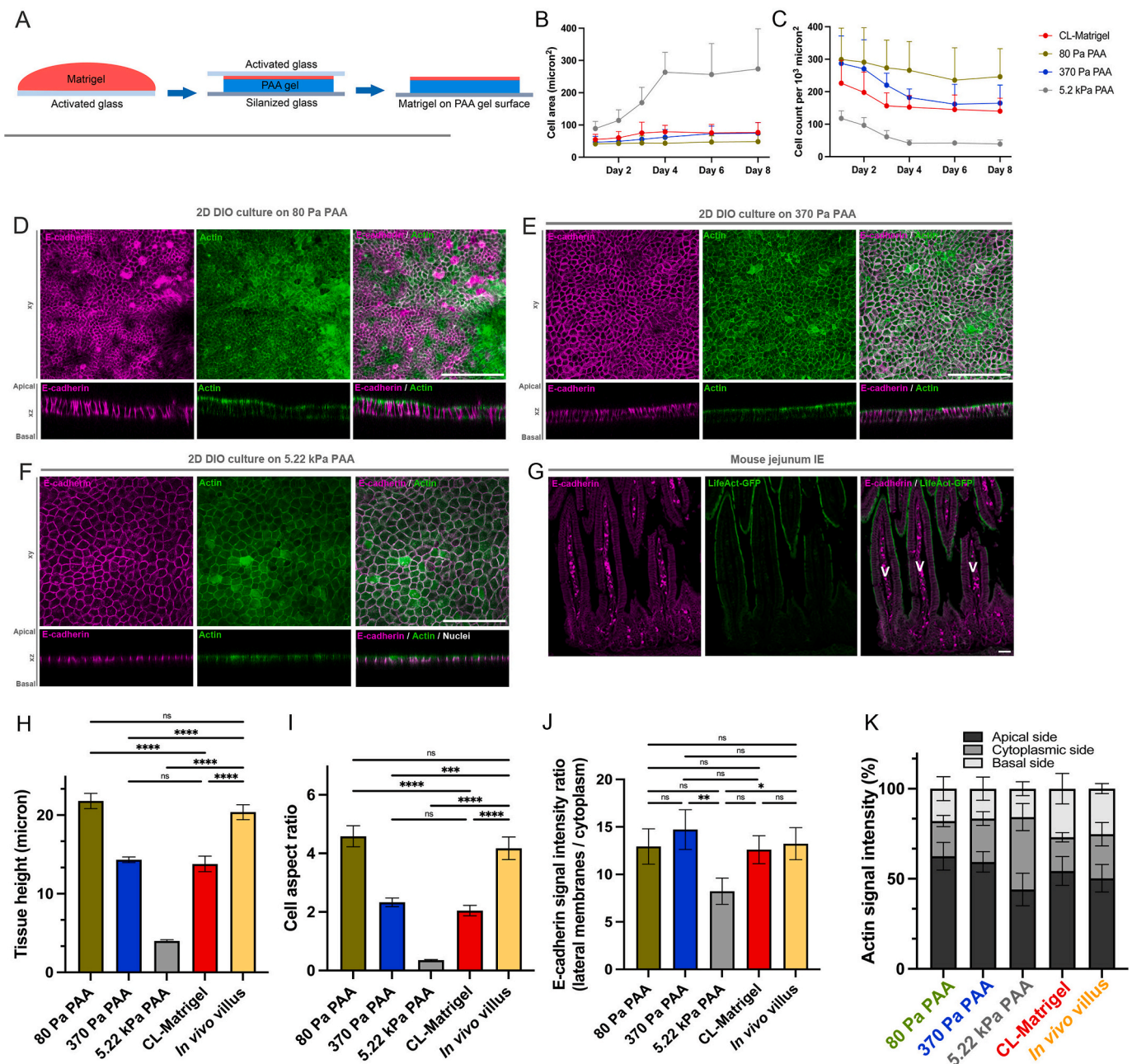


Fig. 3. Culture of DIOs on Matrigel-coated soft hydrogels. **A.** Schematic shows preparation of Matrigel-coated PAA 2D substrates. PAA was polymerized on a Matrigel-coated glass slide (activated glass). After peeling off, a thin Matrigel layer was transferred to the surface of the hydrogel substrate. **B.** Quantification of the variations in cell area on different planar substrates as a function of time. $N = 16$ cells in each time point. Values are mean \pm S.E.M. **C.** Quantification of the variations in cell density on different planar substrates as a function of time. $N = 16$ cells in each time point. Values are mean \pm S.E.M. **D-G.** Confocal analysis of the distribution of E-cadherin (magenta) and actin (green) distribution in DIO cultures on 80 Pa (**D**), 370 Pa (**E**) and 5.22 kPa (**F**) PAA-based substrates, and in mouse jejunum IE (**G**). Both *xy* (*upper panels*) and *xz* (*lower panels*) views are presented. Scale bars **D-F**, 100 μm ; **G**, 30 μm . **H.** Statistical analyses of tissue height on various flat substrates. Mean tissue height (80 Pa PAA) = $21.8 \pm 0.97 \mu\text{m}$, (370 Pa PAA) = $14.33 \pm 0.35 \mu\text{m}$, (5.22 kPa PAA) = $3.99 \pm 0.17 \mu\text{m}$, (*in vivo* villus) = $20.37 \pm 0.96 \mu\text{m}$ $N = 11$ cells for each condition. One-way ANOVA, Tukey's multiple comparisons test, **** $p < 0.0001$. **I.** Statistical analyses of cell aspect ratio (height/width) on various flat substrates. Mean cell aspect ratio (80 Pa PAA) = 4.58 ± 0.36 , (370 Pa PAA) = 2.33 ± 0.15 , (CL-Matrigel) = 2.05 ± 0.18 , (5.22 kPa PAA) = 0.35 ± 0.02 , (*in vivo* villus) = 4.17 ± 0.38 . $N = 11$ cells for each condition. One-way ANOVA, Tukey's multiple comparisons test, *** $p = 0.0002$, **** $p < 0.0001$. **J.** Statistical analyses of the E-cadherin intensity ratio between lateral membranes and the cytoplasm. Mean E-cadherin intensity (80 Pa PAA) = 12.94 ± 1.86 , (370 Pa PAA) = 14.71 ± 2.1 , (5.22 kPa PAA) = 8.22 ± 1.38 , (CL-Matrigel) = 12.6 ± 1.47 , (*in vivo* villus) = 13.23 ± 1.69 . $N = 11$ cells for each condition. Two-way ANOVA, Tukey's multiple comparisons test. * $p = 0.0378$; ** $p = 0.0036$. **K.** Quantification of the percentage of actin fluorescence intensity at the apical, cytoplasm or basal side of DIOs cells cultured on various 2D substrates. $N = 11$ cells for each condition. For each analysis, three independent experiments were carried out.

average cell area in differentiated domains continuously expanded until they reached a plateau (Fig. 3B), regardless of the substrate rigidity. During the first 4 days of culture, while the cell area expanded, the tissue density of the monolayers decreased (Fig. 3C), before reaching a plateau and remained relatively stable until day 8. Although this tendency was observed on the substrates of varying mechanical properties, the development of the differentiated domains in DIO monolayers was impacted by the substrate rigidity. Indeed, after 8-days culture, the average cell areas developed on CL-Matrigel and 370 Pa PAA-Matrigel were 1.5-times larger than those on 80 Pa PAA-Matrigel (mean cell

areas: 74–77 μm^2 for 370 Pa PAA-Matrigel and CL-Matrigel versus 49 μm^2 for 80 Pa PAA-Matrigel, respectively). Moreover, in contrast to the soft gels (80, 370 Pa PAA-Matrigel and CL-Matrigel), the stiffest substrate (5.2 kPa PAA-Matrigel) led to large mean cell areas and loosely packed monolayers (mean cell area: 274 μm^2 and mean cell density: 39 cells per 10,000 μm^2 after 8-days culture). These observations were further confirmed by the analysis of monolayer morphology after 9 days of culture. We found that the DIOs on soft PAA hydrogels adopted densely packed monolayers and columnar cell shape (Fig. 3D–E, H–I) similar to those on CL-Matrigel (Figs. 2J, 3H–I) while on the stiffest

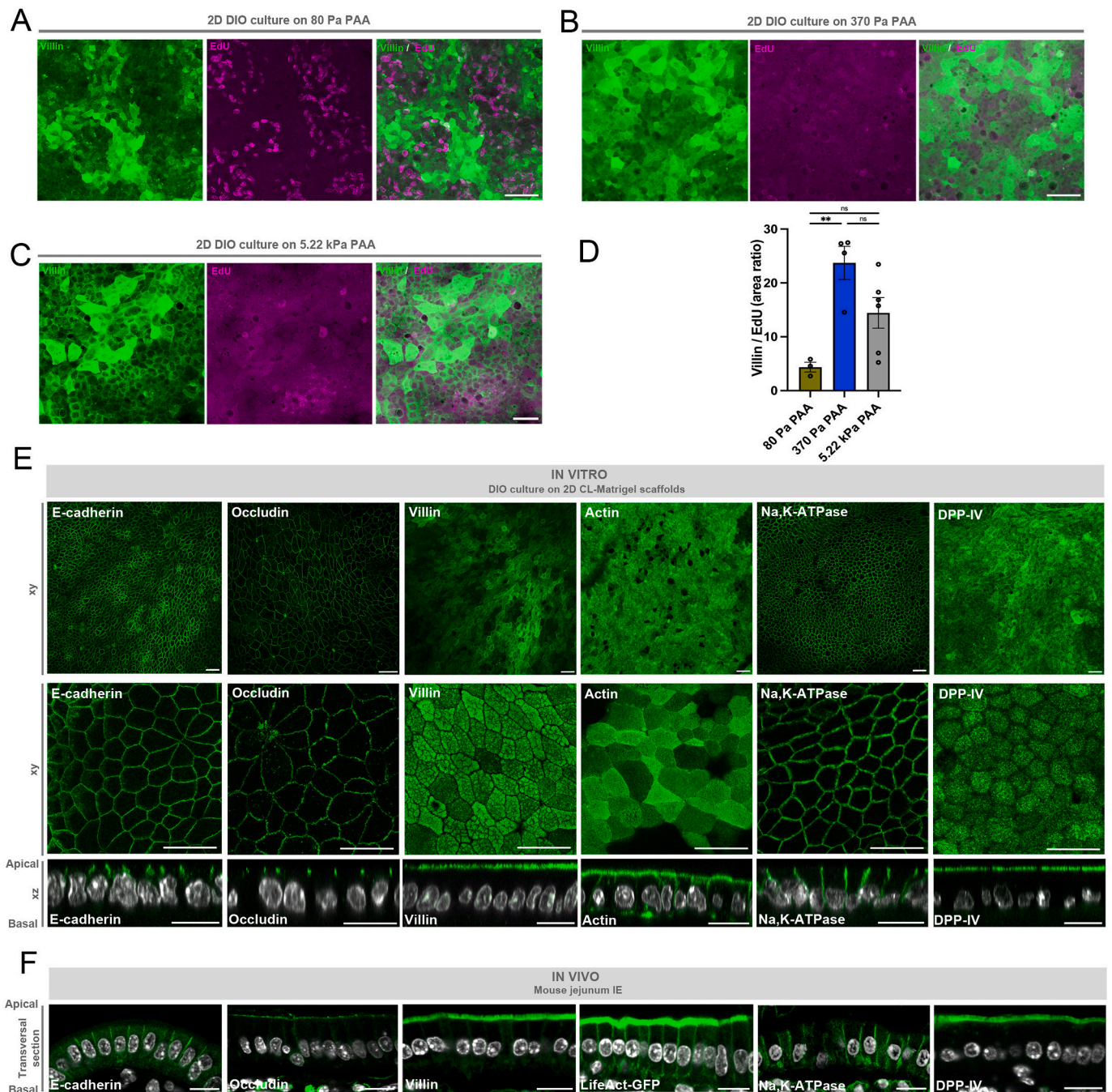


Fig. 4. Enterocytic differentiation in DIOs grown on 2D CL-Matrigel. A–C. Confocal analysis of the distribution of villin (green) and EdU (magenta) distribution in 2D DIO cultures on 80 Pa (A), 370 Pa (B) and 5.22 kPa (C) PAA-based substrates. Scale bars, 30 μm . D. Statistical analysis of the ratio between the surfaces covered by villin-positive cells and by EdU-positive cells. One-way ANOVA, Tukey’s multiple comparisons test, ns non-significant, $**p = 0.0047$. N (80 Pa PAA) = 3, n (370 Pa PAA) = 4, n (5.22 kPa PAA) = 6 samples. Three independent experiments were carried out. E–F. Confocal microscopy analysis of the distribution of E-cadherin, occludin, villin, actin, Na^+, K^+ -ATPase and DPP-IV (green) in 2D DIOs on CL-Matrigel (E) and in transversal sections of mouse jejunum villi (F). In E, both xy (upper panels) and xz (lower panels) views are presented. Nuclei are labelled in gray. Scale bars, 20 μm .

substrate, cells displayed spread and flatten cell shape (Fig. 3F, H-I). In addition, the IE monolayers on CL-Matrigel and 370 Pa PAA-Matrigel resembled closely each other in the cell shape and tissue organization (Figs. 2J and 3E, H-I), indicating that regardless of the nature of the bulky materials, cells regulated tissue architecture mainly according to the substrate stiffness. Interestingly, such hexagonal epithelial cell shapes on the soft gels also resembled those of intestinal villi (Fig. 3G-I), suggesting that the close-to-nature soft substrate favored the development of *in vivo*-like differentiated IE domains.

Immunostainings of key morphologic protein expression further revealed the influence of substrate elasticity on IE properties. Cell cohesiveness was assessed by the localization of E-cadherin, a marker for the *adherens junctions* (AJs). The monolayers on the soft hydrogels showed an optimal lateral distribution of E-cadherin at levels comparable to *in vivo* villi (Figs. 2J, 3D-E, G, J). Moreover, actin signal at cell apical, cytoplasmic and basal portion also demonstrated a similar intensity distribution between the differentiated cells on the soft gels and those on native villi (Figs. 2J and 3G, K). We then sought to determine which stiffness could lead to stable and large differentiated domains in the monolayers. The IE homeostatic state was assessed by villin as a marker of enterocytic differentiation and EdU as a proxy of the proliferative cells (Fig. 4A-C). We found the monolayer on 370 Pa PAA-Matrigel possessed the highest villin/EdU area ratio in comparison with 80 Pa and 5.2 kPa PAA-Matrigel (Fig. 4D). Hence a substrate close to ~400 Pa appeared to be an optimal condition for the development of enterocytic differentiation domains. We noticed that such rigidity was higher than the AFM-determined intestinal ECM rigidity (Fig. 1F). However, protein-protein interactions might be disturbed due to the decellularization process [50]. Moreover, the decellularized ECM lacked modulation by cells and their contractile forces owing to the absence of stromal cells. Thus, such chemical treatment might lead to a weakened ECM with a slightly lower AFM-measured elasticity. To confirm the suitability of CL-Matrigel (~420 Pa) for 2D differentiated IE culture, the differentiation level of DIO monolayers was assessed with the analysis of the expression and distribution of key enterocytic markers (Fig. 4E). In fact, the enterocytic differentiation of 2D DIO monolayers on CL-Matrigel presented a high similarity with villus IE from mouse jejunum (Fig. 4E-F). In both cases, the AJ-associated protein, E-cadherin was concentrated at the upper half of lateral membranes, and occludin, a tight junction component, was found at the upper apical part of cell-cell contacts [51]. Additionally, high density of villin, a brush border marker, was detected exclusively at the apical domain [52,53]. Similarly, actin that is enriched within microvilli as one of the main brush border core proteins was also concentrated at the apical membrane of the cells [52,53]. These suggested that a large number of microvilli covered the differentiated enterocytes on 2D CL-Matrigel as in *in vivo* villi. In contrast, the sodium-potassium pump Na^+/K^+ -ATPase was only localized to the lateral membranes [54,55]. Moreover, these large, planar differentiated domains were distinctly marked with dipeptidyl peptidase-IV (DPP-IV), an intestinal hydrolase responsible for peptide digestion, which is expressed by enterocytes [56]. Globally, the localizations of these protein markers in differentiated zones on CL-Matrigel (Fig. 4E) mirrored those in mouse enterocytes (Fig. 4F), demonstrating that the CL-Matrigel exhibits favourable mechanical stability and substrate stiffness towards enterocytic differentiation.

Hence, substrate mechanical properties could dictate the characteristics of 2D IE monolayers. Our data revealed that an appropriate stiffness window (~100–500 Pa) was required for the formation of an *ex vivo* planar IE with high-density packing and elongated columnar cell shape, reminiscent of *in vivo* tissue. PAA-Matrigel and CL-Matrigel with an elasticity closed to 400 Pa offered the optimal conditions for the formation of enterocytic differentiated domains. Although these soft hydrogel substrates were suitable for the long-term culture of planar IE monolayers, they lack the 3D geometric cues for the formation of crypt-villus micro-architectures.

3.4. Fabrication of 3D scaffolds to mimic crypt-villus axis using CL-Matrigel

We then aimed to transpose DIO monolayer cultures in a suitable 3D microenvironment that reproduced the topography and arrangement of the crypt-villus axis in mouse jejunum [57] (Fig. 5A-B). Previously, similar patterns were made by soft-lithography [18] or 3D-printing technology [19]. Nevertheless, crypt-like structures produced by soft-lithography exhibit flat bottoms with sharp edges and rectangular corners, while the method employing stereolithography relied on expensive and sophisticated machines [18,19]. Here, to address these problems, simplify fabrication and improve yield, we developed a two-steps photolithography process. We firstly produced PDMS stamps with pillars and wells of sharp rectangular edges at the tips and the bottoms (Fig. 5C, 1st – 2nd row), respectively. We then rounded up the sharp edges by curing hemispherical drops of PDMS on the tips and the bottoms by two-steps wet-stamping and remolding. In this way, we obtained a negative PDMS mold with a reverse crypt-villus axis (Fig. 5C, last row). Using the negative mold, we produced positive PDMS replicas, which showed a 3D micropattern consisting of pillars (~350 μm in the height and ~175 μm in the diameter) and wells (~150 μm in the depth and ~100 μm in the diameter) (Fig. 5D). These pillars were laid out by close-packing of equal spheres and each was surrounded by six wells (Fig. 5B). With the PDMS replicas, negative PAA master molds (~55 kPa) were then produced.

Molding soft materials into 3D structures with high aspect ratios is currently a challenge in microengineering. Although often used in microfabrication protocols, PAA material could not be used here as a core component of the 3D culture scaffolds. In practice, soft PAA (~100–500 Pa) could not be shaped into stable 3D microstructures of a high aspect ratio. In addition, while 370 Pa PAA substrates could promote enterocytic differentiation on micro-pillars, the former required an extra step to functionalize a thin layer of Matrigel on its surface for cell adhesion. Moreover, this method caused adhesion between the hydrogel and the mold, and thus failed in generating well-defined 3D crypt-villus axis of high aspect ratio (Fig. 5A-B). Hence, we chose to directly polymerize CL-Matrigel on the 55 kPa PAA negative master molds. Due to their protein repellent surface, these PAA master molds allowed the polymerization and easy unmolding of 3D CL-Matrigel scaffolds. To test the substrate elasticity after the molding process, we probed and compared 3D CL-Matrigel scaffold and 2D CL-Matrigel substrate flatten by flat PAA layers using AFM (Figs. S2A-B). Although slightly increased after the molding procedure (Fig. S2B), the elasticity of 3D CL-Matrigel remained very close to the optimal stiffness window for DIO differentiation and was still at least one order of magnitude lower than reported Collagen I [18] and PEG-DA [19] scaffolds.

3.5. Primary cultures of DIO on 3D CL-Matrigel scaffolds mimic *in vivo* intestinal tissue

DIOs were plated on 3D CL-Matrigel scaffolds and cultured in EM medium. The 3D CL-Matrigel scaffolds remained stable in culture (Fig. S3) and supported the adhesion and expansion of DIOs (Fig. 6A). Indeed, after 21 days of culture, pillars and wells mimicking crypts and villi were lined with a regular cell monolayer (Fig. 6A). Notably, in the 3D DIO cultures, the high density of the brush border markers – actin and villin, was concentrated on the pillars (Fig. 6B, D and E, left panels), resembling villi of mouse jejunum (Fig. 6B, D and E, right panels). *In vivo*, villin is highly expressed in differentiated intestinal cells, i.e., enterocytes [53] and its expression already starts at a low level in progenitor cells [58] (Fig. 6B and E, right panels). This uneven distribution of villin in 3D DIO cultures indicates enterocytes preferentially reside on the pillars. To confirm this, we further stained the *in vitro* 3D DIOs and native tissues with DPP-IV (Figs. S4A-B) and found similar DPP-IV distribution. In short, on 3D CL-Matrigel scaffolds both villin and DPP-IV were more enriched on the pillars than in the wells by about

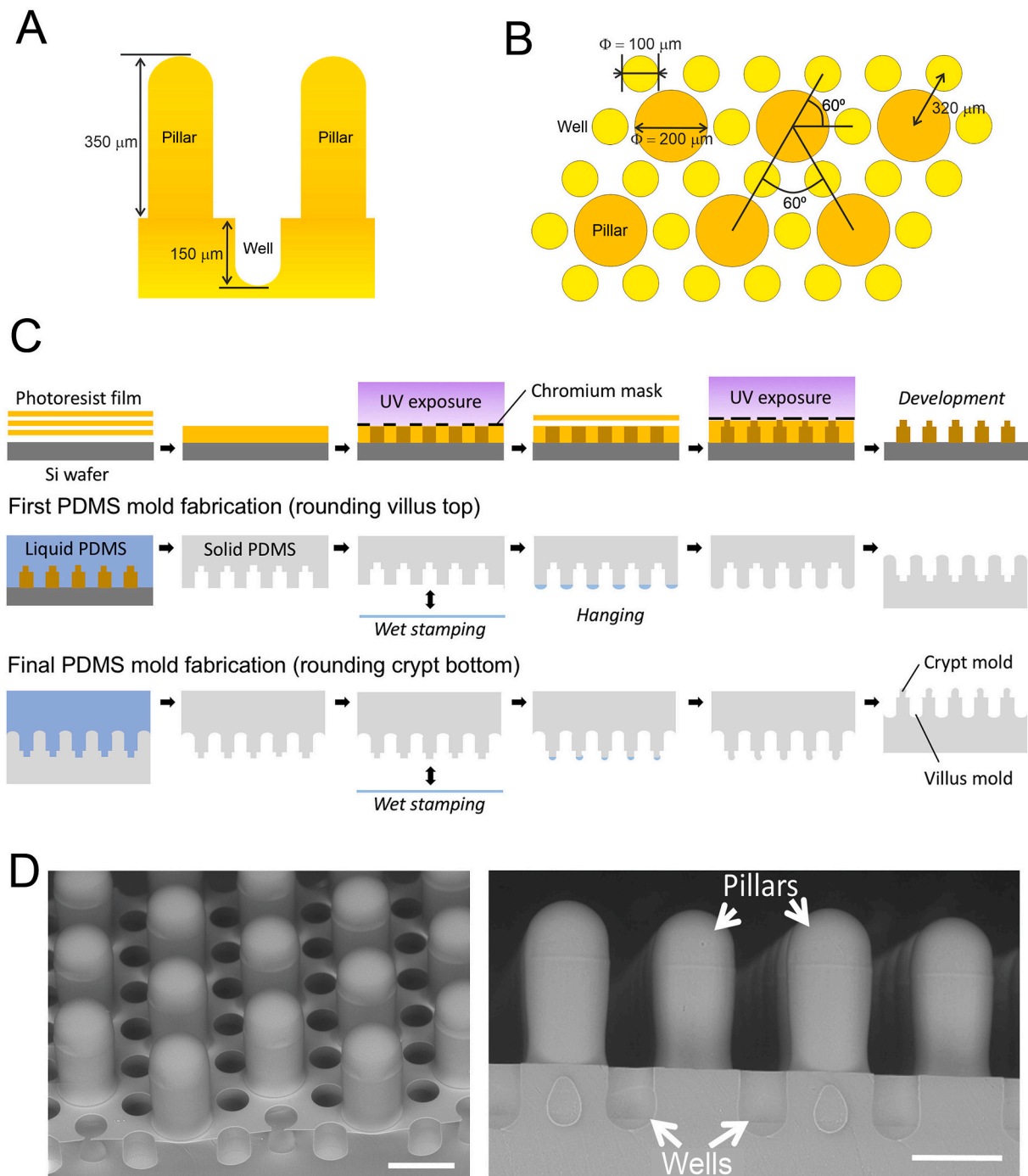
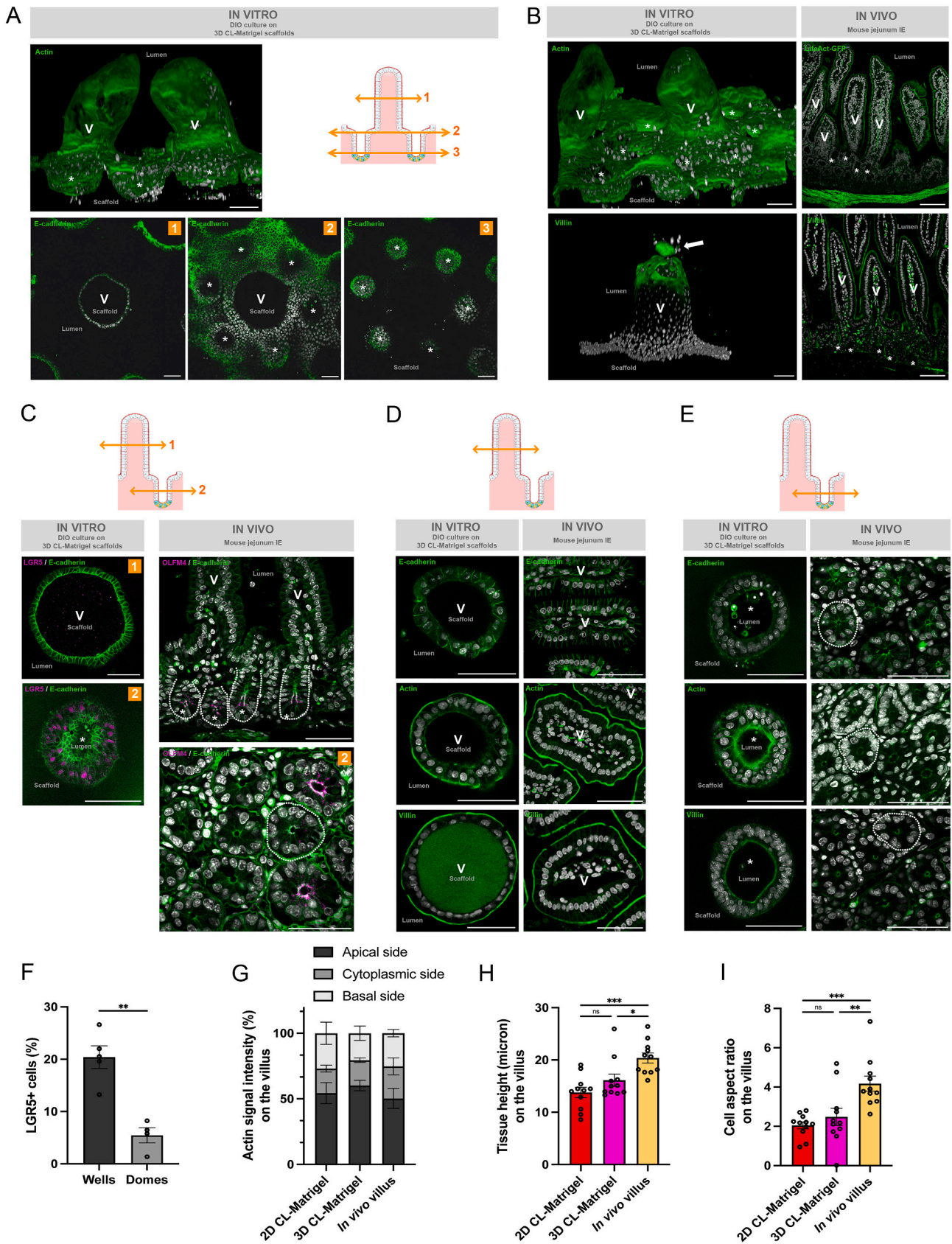


Fig. 5. Fabrication of 3D scaffolds with soft CL-Matrigel to mimic intestinal crypt-villus axis. **A.** Schematic representation of the 3D mimetic scaffold being generated. **B.** Schematic representation of the planar arrangement of pillars and wells in the 3D scaffold being generated. **C.** Schematic of the microfabrication process to produce positive PDMS replica to micromold negative PAA mold. Two-step photolithography was used to produce positive mold in photoresist. This is followed by two molding steps and two wet stamping steps. **D.** SEM images of positive PDMS replicas of the microfabricated 3D crypt-villus axis scaffolds. Scale bars, 200 μm .

1.4–1.6-folds (Fig. S4C), which is comparable to that (1.6–1.7-folds, Fig. S4C) for native tissues. In addition, cells were extruded at the tip of the pillars (white arrow in Fig. 6B, low panel), reproducing epithelial cell shedding that takes place on villi *in vivo* [59,60]. Moreover, ISC detected with LGR5 marker were found to preferentially localize in the wells (Fig. 6C, left panel and 6 F), reminiscent of mouse crypts labelled with OLFM4 marker (Fig. 6C, right panel). To investigate the compartmentalization of different intestinal cells on the 3D scaffolds, we determined the expression of laminins $\alpha 3$ and $\alpha 5$ subunits in the 3D DIO cultures (Fig. S5A). Laminins $\alpha 3$ and $\alpha 5$ are known to be associated with

the villus compartment [61] and could play a role in the differentiation process [62,63]. We found both laminins $\alpha 3$ and $\alpha 5$ were preferentially expressed at the cell base, adjacent to the scaffolds (Fig. S5A). Moreover, similar to villin and DPP-IV, our staining showed an anisotropic distribution of laminins $\alpha 3$ and $\alpha 5$ on the 3D scaffolds with a higher fluorescent intensity concentrated at the pillars than the wells (Fig. S5B). As Matrigel does not contain these laminins, our results suggested the endogenous contribution of the IE to the differentiated villus compartmentalization. Taking together, these data indicate the self-compartmentalization of the proliferative and differentiated regions



(caption on next page)

Fig. 6. DIOs cultured on CL-Matrigel 3D scaffolds mimic the *in vivo* intestinal tissue. **A.** *Upper left panel*, confocal microscopy analysis of the DIOs grown on 3D CL-Matrigel scaffolds for 21 days. Cells were labelled for actin (green) and nuclei (gray). After z-stack acquisition, 3D rendering was generated. V, villus-like structures; *, crypt-like structures. *Upper right panel*, schematic representation of the crypt-villus axis. *Lower panels*, confocal analysis of the DIO monolayer at the level of the villus-like structure (1), the transition between villus and crypts (2) and crypt-like structures (3). Scale bars, 50 μm . **B.** Confocal analysis of brush border markers actin (*upper panels*) and villin (*lower panels*) in DIO cultures on 3D CL-Matrigel scaffolds (*left panels*) and in mouse jejunum IE (*right panels*). White arrow, events of cell extrusion. Scale bars, 50 μm . **C.** *Left panels*, confocal analysis of the stem cell marker LGR5⁺ (magenta) together with E-cadherin (green) at the level of the villus-like (1) or crypt-like (2) structures in DIO cultured on 3D CL-Matrigel scaffolds. *Right panels*, confocal analysis of the stem cell marker OLFM4 (magenta) together with E-cadherin (green) along crypt-villus axis and in crypts (2) in mouse jejunum. White dotted line delimits crypts. Scale bars, 50 μm . **D-E.** Cross-sectional confocal images of E-cadherin, actin and villin at the villi (D) or crypts (E) in DIOs grown on 3D CL-Matrigel scaffolds (*left panels*) or in mouse jejunum (*right panels*). White dotted line delimits crypts. Nuclei are shown in gray. Scale bars, 50 μm . **F.** Statistical analysis of the relative number of Lgr5⁺ cells in the crypt-like or villus-like areas *in vitro*. N = 5 wells, n = 4 domes. Unpaired t-test, **p < 0.01. Two independent experiments were carried out. **G.** Quantification of the percentage of actin fluorescence intensity at the apical, cytoplasm or basal side of cells in different cultures and native tissues. N = 11 cells for each condition. **H.** Statistical analyses of tissue height in various cultures and intestinal tissues. N = 11 cells for each condition. One-way ANOVA, Tukey's multiple comparisons test, ns non-significant, *p < 0.05, ***p < 0.001. **I.** Statistical analyses of cell aspect ratio (height/width) in various cultures and native tissues. N = 11 cells for each condition. One-way ANOVA, Tukey's multiple comparisons test, ns non-significant, **p < 0.01, ***p < 0.001.

on the CL-Matrigel-based 3D scaffolds resembled *in vivo* intestinal tissue. Of note, we could maintain the 3D DIO cultures for as long as 15 weeks in these culture conditions.

Taking a close look at cross-sections of DIO on the pillars (Fig. 6D) and in the wells (Fig. 6E), we found monolayers lining the scaffolds exhibited features of *in vivo* IE tissue. Cells adopted a columnar cell shape as well as a cohesive organization with physiological apical-basal polarity (Fig. 6D–E, left panels and Fig. 6G). We noted that cell height and aspect ratio on the pillars were higher than that on the planar CL-Matrigel substrates and close to the mouse tissue (Fig. 3H–I; 6H–I). Analysis of actin intensity over the pillar cross-sections revealed a high density of actin at the cell apical domain (Fig. 6D, left panels), similar to its *in vivo* counterpart (Fig. 6D, right panels). The distribution of actin intensity over the cells indicated a highly condensed signal at the brush border (Fig. 6D, left panels, and 6G); this was further confirmed by the enrichment of villin and DPP-IV at the same location (Fig. 6D, left panels and Fig. 54). We attributed these epithelial properties to a higher degree of differentiation and physiological-like tissue organization. The effects of 3D geometric on epithelial organization have been studied previously, and it was proposed that 3D curvature is an additional cue besides rigidity for the arrangement of the epithelial tissue [64]. Cells may strengthen AJs to maintain out-of-plan curved topography and thus, leading to a more compressed monolayer with an elongated cell shape [35]. Taken together, our results demonstrate that the soft CL-Matrigel 3D scaffolds promote IE compartmentalization, differentiation and organization that mimic the *in vivo* tissue.

4. Discussion

Herein, we describe a new method to produce Matrigel-based hydrogels that match the physiological elasticity of intestinal tissue. Compared to 2D layers of small patches on pure Matrigel and short-lived IE layers on stiff PDMS substrates, our CL-Matrigel and soft PAA-Matrigel substrates support the long-term culture of self-renewal, compartmentalized and largely expanded IE in 2D format. We analyzed the importance of substrate elasticity in guiding planar intestinal epithelium growth and organization. Firstly, we measured the elasticity of fresh mouse intestinal tissue and ECM by the AFM method (Fig. 1). Our measurement revealed that the intestinal ECM is one order of magnitude softer than previously reported results that were obtained *via* micro-scale testing methods [30]. The AFM measurement provided local mechanical properties that are likely within the mechano-sensing range of cells. Base on this, we produced hydrogels that varied from 80 Pa to 5.2 kPa and, by testing substrates of various elasticities, we identified a narrow mechanical window (~100–500 Pa) required for the formation of a simple columnar differentiated IE. Such IE mimicked many morphological aspects of intestinal tissue. For example, differentiated cells on the soft gels adopt dense packing of highly columnar cells similar to differentiated intestinal cells in villi. This switch from a flat and spread cell shape on the rigid substrate to columnar one could be

due to changes in force balance among tissue contractility, cell-cell interaction and cell-substrate adhesion [35] that are tuned by the substrate rigidity. One could envisage that rigid substrates facilitate the formation of focal adhesions (FAs) that promote cell adherence and cell spreading, resulting in flattened cells. On the other hand, on very soft hydrogel like pure Matrigel, tissue contractility and tension originating from cell-cell junction may overcome weak cell-substrate adhesion [65, 66], preventing cells from spreading and leading to cell layers folding into 3D configurations. Our experimental observations demonstrated a decreasing trend in tissue height and cell aspect ratio on PAA-Matrigel from 5.22 kPa to 80 Pa (Fig. 3H–I), suggesting that cells were subjected to compression as the substrate stiffness decreased. This could be attributed to the mechanical cross-talk between cell-matrix and cell-cell adhesions since soft surfaces could favor cell compaction through downregulation of FAs [65,66]. However, whether there is a sharp threshold of stiffness for epithelial tissue organization and how epithelial cells control their shapes *via* mechano-sensing pathways remain unknown, and the detailed mechanisms deserve further investigations.

The experimental procedure we developed displays diverse advantages. For instance, Matrigel is widely used in cell biology experiments, notably for the 3D cultures of epithelial cells. This hydrogel of natural origin recapitulates the biochemical signature of the basal lamina of epithelia. Its wealth in diverse ECM proteins and growth factors may promote the self-compartmentalization of IE into proliferative and differentiated domains [4,11,15], whereas DIOs on collagen I substrates comprise predominantly proliferative cells which are randomly embedded among other cells [18]. Hence, in contrast to the simple component substrates, the Matrigel-based 3D substrates we developed do not require a series of switches in culture conditions to achieve large, expanded differentiated zones and localized stem cell compartments. Moreover, increasing the cross-linking degree within Matrigel by chemical method lifted its elasticity close to that of intestinal ECM and significantly improve its mechanical stability for IE expansion. Thus, our approach allows the culture of primary IE using a single type of culture medium for the long-term and permits the connection of short-term mechano-sensing and biochemical responses of cells to long-term tissue development and homeostasis.

3D scaffolds, mimicking villus shape and suitable for established cell line cultures, have previously been produced in our lab [64]. Here we have generated soft hydrogel scaffolds consisting of 3D crypt-villus microarchitecture that matches the physiological dimension of villi and crypts in mouse jejunum [18]. In contrast to previous collagen-based 3D scaffolds, our hydrogel scaffolds were at least 10-times softer and thus very close to the mechanical properties of the natural ECM. Although being soft, the 3D CL-Matrigel scaffold was chemically strengthened in its mechanical stability, which supported 3D DIO culture for more than 3 months without significant deformation. This stability also outperforms a recent cross-linked collagen 3D scaffold whose villi are more than 50% shortened by IE after 14-days of culture [67]. We also demonstrated that IE on our scaffolds was fully polarized,

differentiated, and formed *in vivo*-like cell morphology. Surprisingly, the 3D scaffolds alone were sufficient to compartmentalize the proliferative and differentiated cells for LGR5+ cells were preferentially enriched in the wells (Fig. 6F), whereas the villin-positive brush border was concentrated along the pillars (Fig. 6B, D and Fig. S4C). Such compartmentalization took place without any external signals such as biochemical gradients in ECM deposition as well as a soluble morphogenic factor and directed stiffness variations [21]. This may be attributed to a combined effect of endogenous laminins $\alpha 3$ and $\alpha 5$ expression (Fig. S5), physiological rigidities and 3D crypt-villus geometries in regulating cellular signal in IE self-organization and assembly. Indeed, epithelial organizations are known to be responsive to external geometric cues [68,69]. The mechanism underpinned the influence of topographical cues on intestinal cell sorting thus deserves thorough investigations in the future. The simplicity and stability of our platform further enable high-resolution imaging, broad utility in relevant research, *in vitro* toxicology tests for drug screening and high-throughput pre-clinical trials. To conclude, our experimental approach opens novel routes for the development of an *ex vivo* intestinal model for multiple applications in fundamental and translational biological studies.

Credit author statement

Investigation: W.X., J.S., A.Y., B.M., T.D., M.S., S.J., H.W., and D.D. **Methodology:** W.X., J.S., A.Y., C.T., F.L., Y.C. and D.D. **Resources:** A.D., B.R. **Validation, Formal analysis, Visualization:** W.X., J.S. and D.D. **Writing – Original draft:** W.X., J.S., A.Y., C.T., R.M.M., Y.C. and D.D. **Writing – Review and editing:** W.X. and D.D. **Conceptualization:** W.X. and D.D. **Supervision, Project administration and funding acquisition:** D.D.

Data availability

The data supporting the findings of this study are available from the corresponding author upon request.

Declaration of competing interest

The authors declare that they have no known competing financial interests or personal relationships that could have appeared to influence the work reported in this paper.

Acknowledgments

We thank Dr. Benoit Ladoux for his helpful discussions. We thank Virginie Bazin and Michael Trichet for technical help in scanning electron microscopy analyses (Electron Microscopy facility, Institut de Biologie Paris-Seine (IBPS)). Confocal microscopy was performed in the ImagoSeine facility (Institut Jacques Monod, IJM), member of the France BioImaging infrastructure supported by the French National Research Agency (ANR-10-INSB-04, «Investments for the future»), with the help of Xavier Baudin, Paul Lambert and Nicolas Moisan. We acknowledge the technical platform and animal core facility “Buffon” of the Université de Paris/IJM, especially Isabelle Le Parco, Angélique Dauvin, Ludovic Maingault, Florianne Michel, Laetitia Pontoizeau and Daniel Quintas for animals’ care. This work was supported by grants from PRESTIGE co-financing grant #PRESTIGE-2016-4-0007 (W.X.), Marie Skłodowska-Curie Actions #846449 (W.X.), the “Institut Pierre-Gilles de Gennes” (laboratoire d’excellence, “Investissements d’avenir” program ANR-10-IDEX-0001-02 PSL and ANR-10-LABX-31.) (to A. Y and Y.C.), the Mission for Transversal and Interdisciplinary Initiatives (MiTi, CNRS) – Biomimetic Challenge 2019 (to A.Y., Y.C. and D.D.), the Groupama Foundation – Research Prize for Rare Diseases 2017 (to D. D.), the LabEx “Who Am I?” #ANR-11-LABX-0071 and the Université de Paris IdEx #ANR-18-IDEX-0001 funded by the French Government through its “Investments for the Future” program (to B.R and D. D), and

the Human Frontier Science Program (RGP0038/2018) (to D. D).

Appendix A. Supplementary data

Supplementary data to this article can be found online at <https://doi.org/10.1016/j.biomaterials.2022.121380>.

References

- [1] H. Gehart, H. Clevers, Tales from the crypt: new insights into intestinal stem cells, *Nat. Rev. Gastroenterol. Hepatol.* 16 (1) (2019) 19–34.
- [2] C. Crosnier, D. Stamataki, J. Lewis, Organizing cell renewal in the intestine: stem cells, signals and combinatorial control, *Nat. Rev. Genet.* 7 (5) (2006) 349–359.
- [3] F. Schutgens, H. Clevers, Human organoids: tools for understanding biology and treating diseases, *Annu. Rev. Pathol.* 15 (1) (2020) 211–234.
- [4] T. Sato, R.G. Vries, H.J. Snippert, M. van de Wetering, N. Barker, D.E. Stange, J. H. van Es, A. Abo, P. Kujala, P.J. Peters, H. Clevers, Single Lgr5 stem cells build crypt-villus structures *in vitro* without a mesenchymal niche, *Nature* 459 (7244) (2009) 262–265.
- [5] T. Sato, J.H. van Es, H.J. Snippert, D.E. Stange, R.G. Vries, M. van den Born, N. Barker, N.F. Shroyer, M. van de Wetering, H. Clevers, Paneth cells constitute the niche for Lgr5 stem cells in intestinal crypts, *Nature* 469 (7330) (2011) 415–418.
- [6] G. Rossi, A. Manfrin, M.P. Lutolf, Progress and potential in organoid research, *Nat. Rev. Genet.* 19 (11) (2018) 671–687.
- [7] N. Shanks, R. Greek, J. Greek, Are animal models predictive for humans? *Philos. Ethics Humanit. Med.* 4 (1) (2009) 2.
- [8] C.A. Larregieu, L.Z. Benet, Drug discovery and regulatory considerations for improving *in silico* and *in vitro* predictions that use caco-2 as a surrogate for human intestinal permeability measurements, *AAPS J.* 15 (2) (2013) 483–497.
- [9] J.G. In, J. Foulke-Abel, M.K. Estes, N.C. Zachos, O. Kovbasnjuk, M. Donowitz, Human mini-guts: new insights into intestinal physiology and host–pathogen interactions, *Nat. Rev. Gastroenterol. Hepatol.* 13 (11) (2016) 633–642.
- [10] T. Sato, H. Clevers, Growing self-organizing mini-guts from a single intestinal stem cell: mechanism and applications, *Science* 340 (6137) (2013) 1190–1194.
- [11] J.R. Spence, C.N. Mayhew, S.A. Rankin, M.F. Kuhar, J.E. Vallance, K. Tolle, E. E. Hoskins, V.V. Kalinichenko, S.I. Wells, A.M. Zorn, N.F. Shroyer, J.M. Wells, Directed differentiation of human pluripotent stem cells into intestinal tissue *in vitro*, *Nature* 470 (7332) (2011) 105–109.
- [12] X. Yin, Benjamin E. Mead, H. Safaee, R. Langer, Jeffrey M. Karp, O. Levy, Engineering stem cell organoids, *Cell Stem Cell* 18 (1) (2016) 25–38.
- [13] Z. Jabaji, C.M. Sears, G.J. Brinkley, N.Y. Lei, V.S. Joshi, J. Wang, M. Lewis, M. Stelzner, M.G. Martín, J.C.Y. Dunn, Use of collagen gel as an alternative extracellular matrix for the *in vitro* and *in vivo* growth of murine small intestinal epithelium, *Tissue Eng. C Methods* 19 (12) (2013) 961–969.
- [14] Y. Liu, Z. Qi, X. Li, Y. Du, Y.-G. Chen, Monolayer culture of intestinal epithelium sustains Lgr5+ intestinal stem cells, *Cell Discovery* 4 (1) (2018) 32.
- [15] C.A. Thorne, I.W. Chen, L.E. Sanman, M.H. Cobb, L.F. Wu, S.J. Altschuler, Enteroid monolayers reveal an autonomous WNT and BMP circuit controlling intestinal epithelial growth and organization, *Dev. Cell* 44 (5) (2018) 624–633, e4.
- [16] C. Moon, K.L. VanDussen, H. Miyoshi, T.S. Stappenbeck, Development of a primary mouse intestinal cell monolayer culture system to evaluate factors that modulate IgA transcytosis, *Mucosal Immunol.* 7 (4) (2014) 818–828.
- [17] G. Altay, E. Larrañaga, S. Tosi, F.M. Barriga, E. Batlle, V. Fernández-Majada, E. Martínez, Self-organized intestinal epithelial monolayers in crypt and villus-like domains show effective barrier function, *Sci. Rep.* 9 (1) (2019) 10140.
- [18] Y. Wang, D.B. Gunasekara, M.I. Reed, M. DiSalvo, S.J. Bultman, C.E. Sims, S. T. Magness, N.L. Allbritton, A microengineered collagen scaffold for generating a polarized crypt-villus architecture of human small intestinal epithelium, *Biomaterials* 128 (2017) 44–55.
- [19] J. Creff, R. Courson, T. Mangeat, J. Foncy, S. Souleille, C. Thibault, A. Besson, L. Malaquin, Fabrication of 3D scaffolds reproducing intestinal epithelium topography by high-resolution 3D stereolithography, *Biomaterials* 221 (2019) 119404.
- [20] S.R. Merker, J. Weitz, D.E. Stange, Gastrointestinal organoids: how they gut it out, *Dev. Biol.* 420 (2) (2016) 239–250.
- [21] Y. Wang, R. Kim, S.S. Hinman, B. Zwarycz, S.T. Magness, N.L. Allbritton, Bioengineered systems and designer matrices that recapitulate the intestinal stem cell niche, *CMGH Cell. Mol. Gastroenterol. Hepatol.* 5 (3) (2018) 440–453.e1.
- [22] H.F. Farin, I. Jordens, M.H. Mosa, O. Basak, J. Korving, D.V.F. Tauriello, K. de Punder, S. Angers, P.J. Peters, M.M. Maurice, H. Clevers, Visualization of a short-range Wnt gradient in the intestinal stem-cell niche, *Nature* 530 (7590) (2016) 340–343.
- [23] D.-Y. Chen, J. Crest, S.J. Streichan, D. Bilder, Extracellular matrix stiffness cues junctional remodeling for 3D tissue elongation, *Nat. Commun.* 10 (1) (2019) 3339.
- [24] E.H. Barriga, K. Franze, G. Charras, R. Mayor, Tissue stiffening coordinates morphogenesis by triggering collective cell migration *in vivo*, *Nature* 554 (2018) 523–527.
- [25] D.C. Stewart, D. Berrie, J. Li, X. Liu, C. Rickerson, D. Mkoji, A. Iqbal, S. Tan, A. L. Doty, S.C. Glover, C.S. Simmons, Quantitative assessment of intestinal stiffness and associations with fibrosis in human inflammatory bowel disease, *PLoS One* 13 (7) (2018), e0200377.
- [26] G. Latella, F. Rieder, Intestinal fibrosis: ready to be reversed, *Curr. Opin. Gastroenterol.* 33 (4) (2017) 239–245.

- [27] M. Kedinger, J.-N. Freund, J.-F. Launay, P. Simon-Assmann, Cell interactions through the basement membrane in intestinal development and differentiation, in: I.R. Sanderson, W.A. Walker (Eds.), *Development of the Gastrointestinal Tract*, PMPH-USA, 2000, pp. 83–102.
- [28] D.P. Sokolis, S.G. Sassani, Microstructure-based constitutive modeling of the large intestine validated by histological observations, *J. Mech. Behav. Biomed. Mater.* 21 (2013) 149–166.
- [29] I. Leivo, T. Tani, L. Laitinen, R. Bruns, E. Kivilaakso, V.P. Lehto, R.E. Burgeson, I. Virtanen, Anchoring complex components laminin-5 and type VII collagen in intestine: association with migrating and differentiating enterocytes, *J. Histochem. Cytochem.* 44 (11) (1996) 1267–1277.
- [30] S.N. Steinway, J. Saleh, B.-K. Koo, D. Delacour, D.-H. Kim, Human microphysiological models of intestinal tissue and gut microbiome, *Front. Bioeng. Biotechnol.* 8 (725) (2020).
- [31] A.M. Handorf, Y. Zhou, M.A. Halanski, W.J. Li, Tissue stiffness dictates development, homeostasis, and disease progression, *Organogenesis* 11 (1) (2015) 1–15.
- [32] W. Xi, T.B. Saw, D. Delacour, C.T. Lim, B. Ladoux, Material approaches to active tissue mechanics, *Nat. Rev. Mater.* 4 (1) (2019) 23–44.
- [33] Y. Wang, M. DiSalvo, D.B. Gunasekara, J. Dutton, A. Proctor, M.S. Lebhara, I. A. Williamson, J. Speer, R.L. Howard, N.M. Smiddy, S.J. Bultman, C.E. Sims, S. T. Magness, N.L. Allbritton, Self-renewing monolayer of primary colonic or rectal epithelial cells, CMGH cell, *Mol. Gastroenterol. Hepatol.* 4 (1) (2017) 165–182, e7.
- [34] N. Gjorevski, N. Sachs, A. Manfrin, S. Giger, M.E. Bragina, P. Ordóñez-Morán, H. Clevers, M.P. Lutolf, Designer matrices for intestinal stem cell and organoid culture, *Nature* 539 (2016) 560–564.
- [35] E. Hannezo, J. Prost, J.-F. Joanny, Theory of epithelial sheet morphology in three dimensions, *Proc. Natl. Acad. Sci. U. S. A.* 111 (1) (2014) 27–32.
- [36] L. Li, J. Eyckmans, C.S. Chen, Designer biomaterials for mechanobiology, *Nat. Mater.* 16 (2017) 1164.
- [37] Z. Tong, K. Martyn, A. Yang, X. Yin, B.E. Mead, N. Joshi, N.E. Sherman, R. S. Langer, J.M. Karp, Towards a defined ECM and small molecule based monolayer culture system for the expansion of mouse and human intestinal stem cells, *Biomaterials* 154 (2018) 60–73.
- [38] S. Yui, T. Nakamura, T. Sato, Y. Nemoto, T. Mizutani, X. Zheng, S. Ichinose, T. Nagaishi, R. Okamoto, K. Tsuchiya, H. Clevers, M. Watanabe, Functional engraftment of colon epithelium expanded in vitro from a single adult Lgr5+ stem cell, *Nat. Med.* 18 (4) (2012) 618–623.
- [39] M. Saitou, Y. Ando-Akatsuka, M. Itoh, M. Furuse, J. Inazawa, K. Fujimoto, S. Tsukita, Mammalian occludin in epithelial cells: its expression and subcellular distribution, *Eur. J. Cell Biol.* 73 (3) (1997) 222–231.
- [40] J. Riedl, A.H. Crevenna, K. Kessenbrock, J.H. Yu, D. Neukirchen, M. Bista, F. Bradke, D. Jenne, T.A. Holak, Z. Werb, M. Sixt, R. Wedlich-Soldner, Lifeact: a versatile marker to visualize F-actin, *Nat. Methods* 5 (7) (2008) 605–607.
- [41] H. Miyoshi, T.S. Stappenbeck, In vitro expansion and genetic modification of gastrointestinal stem cells in spheroid culture, *Nat. Protoc.* 8 (12) (2013) 2471–2482.
- [42] S.V. Plotnikov, B. Sabass, U.S. Schwarz, C.M. Waterman, Chapter 20 - high-resolution traction force microscopy, in: J.C. Waters, T. Wittman (Eds.), *Methods in Cell Biology*, Academic Press, 2014, pp. 367–394.
- [43] G. Totonelli, P. Maghsoudlou, M. Garriboli, J. Riegler, G. Orlando, A.J. Burns, N. J. Sebire, V.V. Smith, J.M. Fishman, M. Ghionzoli, M. Turmaine, M.A. Birchall, A. Atala, S. Soker, M.F. Lythgoe, A. Seifalian, A. Pierro, S. Eaton, P. De Coppi, A rat decellularized small bowel scaffold that preserves villus-crypt architecture for intestinal regeneration, *Biomaterials* 33 (12) (2012) 3401–3410.
- [44] D. Delacour, A. Koch, W. Ackermann, I.E.-L. Parco, H.-P. Elsässer, F. Poirier, R. Jacob, Loss of galectin-3 impairs membrane polarisation of mouse enterocytes in vivo, *J. Cell Sci.* 121 (4) (2008) 458–465.
- [45] J. Magescas, L. Sengmanivong, A. Viau, A. Mayeux, T. Dang, M. Burtin, U. J. Nilsson, H. Leffler, F. Poirier, F. Terzi, D. Delacour, Spindle pole cohesion requires glycosylation-mediated localization of NuMA, *Sci. Rep.* 7 (1) (2017) 1474.
- [46] R. Akhtar, M.J. Sherratt, J.K. Cruickshank, B. Derby, Characterizing the elastic properties of tissues, *Mater. Today* 14 (3) (2011) 96–105.
- [47] L.A. Johnson, E.S. Rodansky, K.L. Sauder, J.C. Horowitz, J.D. Mih, D. J. Tschumperlin, P.D. Higgins, Matrix stiffness corresponding to strictured bowel induces a fibrogenic response in human colonic fibroblasts, *Inflamm. Bowel Dis.* 19 (5) (2013) 891–903.
- [48] T. Sato, H. Clevers, Growing self-organizing mini-guts from a single intestinal stem cell: mechanism and applications, *Science* 340 (6137) (2013) 1190–1194.
- [49] R.J. Pelham, Y.-I. Wang, Cell locomotion and focal adhesions are regulated by substrate flexibility, *Proc. Natl. Acad. Sci. U.S.A.* 94 (25) (1997) 13661–13665.
- [50] J.W. Goding, 10 - analysis of antigens recognized by monoclonal antibodies, in: J. W. Goding (Ed.), *Monoclonal Antibodies*, third ed., Academic Press, London, 1996, pp. 234–326.
- [51] B. Lee, K.M. Moon, C.Y. Kim, Tight junction in the intestinal epithelium: its association with diseases and regulation by phytochemicals, *J. Immunol. Res.* 2018 (2018) 2645465.
- [52] D. Louvard, The function of the major cytoskeletal components of the brush border, *Curr. Opin. Cell Biol.* 1 (1) (1989) 51–57.
- [53] D. Delacour, J. Salomon, S. Robine, D. Louvard, Plasticity of the brush border — the yin and yang of intestinal homeostasis, *Nat. Rev. Gastroenterol. Hepatol.* 13 (3) (2016) 161–174.
- [54] J.H. Kaplan, Biochemistry of Na,K-ATPase, *Annu. Rev. Biochem.* 71 (2002) 511–535.
- [55] M.A. Rocafull, L.E. Thomas, J.R. del Castillo, The second sodium pump: from the function to the gene, *Pflug. Arch. Eur. J. Physiol.* 463 (6) (2012) 755–777.
- [56] J.P. Gorvel, A. Ferrero, L. Chambraud, A. Rigal, J. Bonicel, S. Maroux, Expression of sucrase-isomaltase and dipeptidylpeptidase IV in human small intestine and colon, *Gastroenterology* 101 (3) (1991) 618–625.
- [57] M. Bjerknes, H. Cheng, Methods for the isolation of intact epithelium from the mouse intestine, *Anat. Rec.* 199 (4) (1981) 565–574.
- [58] F. El Marjou, K.-P. Janssen, B. Hung-Junn Chang, M. Li, V. Hindie, L. Chan, D. Louvard, P. Chambon, D. Metzger, S. Robine, Tissue-specific and inducible Cre-mediated recombination in the gut epithelium, *Genesis* 39 (3) (2004) 186–193.
- [59] T.F. Bullen, S. Forrest, F. Campbell, A.R. Dodson, M.J. Hershman, D.M. Pritchard, J.R. Turner, M.H. Montrose, A.J.M. Watson, Characterization of epithelial cell shedding from human small intestine, *Lab. Invest.* 86 (10) (2006) 1052–1063.
- [60] J.M. Williams, C.A. Duckworth, M.D. Burkitt, A.J. Watson, B.J. Campbell, D. M. Pritchard, Epithelial cell shedding and barrier function: a matter of life and death at the small intestinal villus tip, *Vet. Pathol.* 52 (3) (2015) 445–455.
- [61] M. Antfolk, K.B. Jensen, A bioengineering perspective on modelling the intestinal epithelial physiology in vitro, *Nat. Commun.* 11 (1) (2020) 6244.
- [62] I.C. Teller, J. Auclair, E. Herring, R. Gauthier, D. Ménard, J.-F. Beaulieu, Laminins in the developing and adult human small intestine: relation with the functional absorptive unit, *Dev. Dynam.* 236 (7) (2007) 1980–1990.
- [63] I.C. Teller, J.F. Beaulieu, Interactions between laminin and epithelial cells in intestinal health and disease, *Exp. Rev. Mol. Med.* 3 (24) (2001) 1–18.
- [64] J. Salomon, C. Gaston, J. Magescas, B. Duvauchelle, D. Canioni, L. Sengmanivong, A. Mayeux, M. G. C. F. L. J. V. J. P. F. M. N. S. J. B. N. L. B. G. O. D. Delacour, Contractile forces at tricellular contacts modulate epithelial organization and monolayer integrity, *Nat. Commun.* 8 (2017) 13998.
- [65] W.H. Guo, M.T. Frey, N.A. Burnham, Y.L. Wang, Substrate rigidity regulates the formation and maintenance of tissues, *Biophys. J.* 90 (6) (2006) 2213–2220.
- [66] H.E. Balcioğlu, L. Balasubramaniam, T.V. Stirbat, B.L. Doss, M.-A. Fardin, R.-M. Mège, B. Ladoux, A subtle relationship between substrate stiffness and collective migration of cell clusters, *Soft Matter* 16 (7) (2020) 1825–1839.
- [67] M. Verhulsel, A. Simon, M. Bernheim-Dennery, V.R. Gannavarapu, L. Gérémie, D. Ferraro, D. Krndija, L. Talini, J.-L. Viovy, D.M. Vignjevic, S. Descroix, Developing an advanced gut on chip model enabling the study of epithelial cell/fibroblast interactions, *Lab Chip* 21 (2) (2021) 365–377.
- [68] W. Xi, S. Sonam, T.B. Saw, B. Ladoux, C.T. Lim, Emergent patterns of collective cell migration under tubular confinement, *Nat. Commun.* 8 (1) (2017) 1517.
- [69] H.G. Yevick, G. Duclos, I. Bonnet, P. Silberzan, Architecture and migration of an epithelium on a cylindrical wire, *Proc. Natl. Acad. Sci. U. S. A.* 112 (19) (2015) 5944–5949.